Kobe University Repository : Kernel

PDF issue: 2025-12-05

Semaphorin 3G Provides a Repulsive Guidance Cue to Lymphatic Endothelial Cells via Neuropilin-2/PlexinD1

Liu, Xinyi
Uemura, Akiyoshi
Fukushima, Yoko
Yoshida, Yutaka
Hirashima, Masanori

(Citation)
Cell Reports,17(9):2299-2311

(Issue Date)
2016-11-22

(Resource Type)
journal article

(Version)
Version of Record

(Rights)
©2016 The Authors.
This is an open access article under the CC BY-NC-ND license
(http://creativecommons.org/licenses/by-nc-nd/4.0/)

(URL)
https://hdl.handle.net/20.500.14094/90003771

Cell Reports

Article

Semaphorin 3G Provides a Repulsive Guidance Cue to Lymphatic Endothelial Cells via Neuropilin-2/PlexinD1

Graphical Abstract

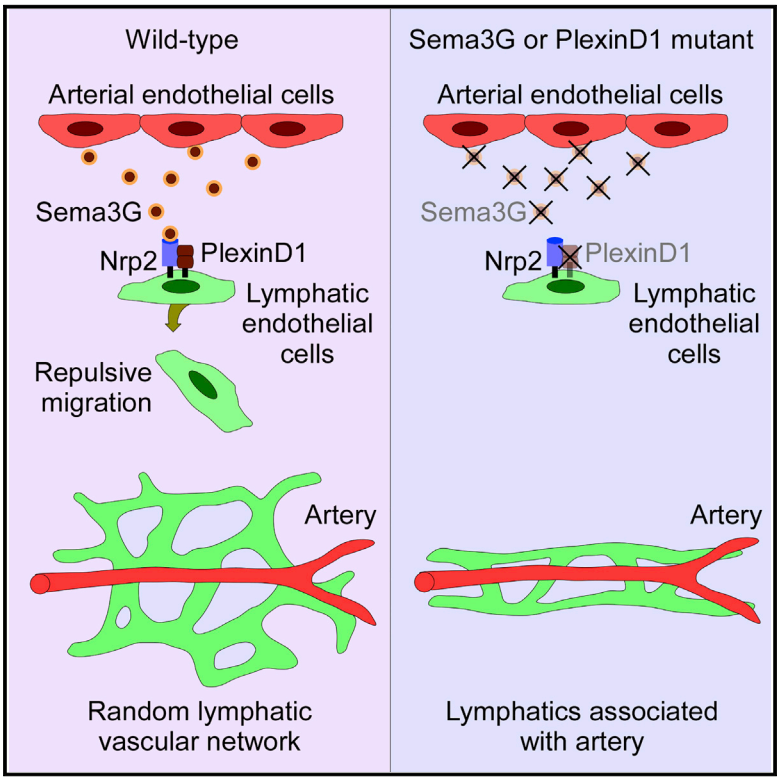

Authors

Xinyi Liu, Akiyoshi Uemura, Yoko Fukushima, Yutaka Yoshida, Masanori Hirashima

Correspondence

mhirashi@med.kobe-u.ac.jp

In Brief

During dermal lymphatic vascular development, the distribution of lymphatic endothelial cells is regulated by guidance cues from blood vessels. Liu et al. show that an artery-derived ligand, Sema3G, acts as a repulsive guidance cue through the Nrp2/PlexinD1 receptor complex to regulate lymphatic vascular patterning in mouse embryonic skin.

Highlights

- PlexinD1- or Sema3G-deficient mouse embryos show abnormal artery-lymph alignment
- PlexinD1 in lymphatic endothelial cells is crucial for proper vascular patterning
- Sema3G acts as a repulsive guidance cue through the Nrp2/PlexinD1 receptor complex

Liu et al., 2016, Cell Reports *17*, 2299–2311
November 22, 2016 © 2016 The Author(s).
http://dx.doi.org/10.1016/j.celrep.2016.11.008

Cell Reports
Article

OPEN ACCESS
CellPress

Semaphorin 3G Provides a Repulsive Guidance Cue to Lymphatic Endothelial Cells via Neuropilin-2/PlexinD1

Xinyi Liu,[1] Akiyoshi Uemura,[2] Yoko Fukushima,[3] Yutaka Yoshida,[4] and Masanori Hirashima[1,5,*]
[1]Division of Vascular Biology, Department of Physiology and Cell Biology, Kobe University Graduate School of Medicine, 7-5-1 Kusunoki-cho, Chuo-ku, Kobe, Hyogo 650-0017, Japan
[2]Department of Retinal Vascular Biology, Nagoya City University Graduate School of Medical Sciences, 1 Kawasumi Mizuho-cho, Mizuho-ku, Nagoya 467-8601, Japan
[3]Department of Ophthalmology, Graduate School of Medicine, Osaka University, 2-2 Yamadaoka, Suita, Osaka 565-0871, Japan
[4]Division of Developmental Biology, Cincinnati Children's Hospital Medical Center, 3333 Burnet Avenue, Cincinnati, OH 45229, USA
[5]Lead Contact
*Correspondence: mhirashi@med.kobe-u.ac.jp
http://dx.doi.org/10.1016/j.celrep.2016.11.008

SUMMARY

The vertebrate circulatory system is composed of closely related blood and lymphatic vessels. It has been shown that lymphatic vascular patterning is regulated by blood vessels during development, but its molecular mechanisms have not been fully elucidated. Here, we show that the artery-derived ligand semaphorin 3G (Sema3G) and the endothelial cell receptor PlexinD1 play a role in lymphatic vascular patterning. In mouse embryonic back skin, genetic inactivation of Sema3G or PlexinD1 results in abnormal artery-lymph alignment and reduced lymphatic vascular branching. Conditional ablation in mice demonstrates that PlexinD1 is primarily required in lymphatic endothelial cells (LECs). In vitro analyses show that Sema3G binds to neuropilin-2 (Nrp2), which forms a receptor complex with PlexinD1. Sema3G induces cell collapse in an Nrp2/PlexinD1-dependent manner. Our findings shed light on a molecular mechanism by which LECs are distributed away from arteries and form a branching network during lymphatic vascular development.

INTRODUCTION

The vertebrate circulatory system comprises blood and lymphatic vascular systems. The developmental and anatomical associations between these two vascular systems are crucial for integrated vascular function. Blood endothelial cells (BECs) are derived from the nascent mesodermal cells and form a closed and hierarchical structure of arteries, veins, and capillaries. The molecular mechanisms underlying arterial or venous endothelial specification have been analyzed intensively, and signaling pathways such as vascular endothelial growth factor A (VEGF-A) and Dll/Notch have been implicated in this process (Benedito et al., 2009; Swift and Weinstein, 2009). Lymphatic endothelial cells (LECs) are differentiated from venous endothelial cells by expression of the transcription factors Sox18 and Prox1 (François et al., 2008; Srinivasan et al., 2007; Wigle et al., 2002) and form a blind-end and unidirectional system of lymphatic capillaries and collecting lymphatic vessels (Tammela and Alitalo, 2010). Lymphatic capillaries form a random network in peripheral tissues, such as the skin, whereas collecting lymphatic vessels are anatomically localized in parallel with arteries and eventually connect to veins at the venous angle (Sabin, 1902, 1904). During lymphatic vessel formation, VEGF-C plays a critical role in LEC proliferation, migration, and survival (Karkkainen et al., 2004). Recent studies indicated that lymphatic vascular patterning is regulated, at least in part, by blood vessels that develop earlier than lymphatic vessels (Hägerling et al., 2013). The molecular mechanisms underlying the spatial interaction between arteries and lymphatics have been elucidated by studies in zebrafish embryos showing that Cxcr4$^+$ LECs migrate adjacent to trunk arterial intersegmental blood vessels, which depends on the release of chemokine Cxcl12 from arteries (Bussmann et al., 2010; Cha et al., 2012; Yaniv et al., 2006). A recent study in mouse embryos showed that the formation of lymphatic vessel depends on arteriogenesis regulated by Pitx2 and its target gene, Cxcl12, in the dorsal mesentery (Mahadevan et al., 2014). Following migration along arteries, LECs should eventually be repelled from blood vessels to form a random lymphatic vascular network in the peripheral tissues. However, little is known about which factors provide the repulsive guidance cues from arteries to LECs.

Several factors have been shown to serve as repulsive guidance cues in endothelial cells (Adams and Eichmann, 2010; Meadows and Cleaver, 2015). The class 3 semaphorins (Sema3s) represent a family of secreted factors characterized by a conserved semaphorin domain and have been implicated in a variety of functions, including axon guidance, cell migration, growth cone collapse, and vascular development (Gurrapu and Tamagnone, 2016; Jongbloets and Pasterkamp, 2014; Koropouli and Kolodkin, 2014; Kumanogoh and Kikutani, 2013; Tran et al., 2007; Yoshida, 2012). Most of these effects are mediated by plexins, large transmembrane receptors with highly conserved cytoplasmic domains, and co-receptors such as

This is an open access article under the CC BY-NC-ND license (http://creativecommons.org/licenses/by-nc-nd/4.0/).

neuropilins (Nrp) (Chen et al., 1997; Takahashi et al., 1998). Several lines of evidence demonstrate that the Sema3E/PlexinD1 axis plays a crucial role in blood vessel patterning (Gitler et al., 2004; Gu et al., 2005; Meadows et al., 2012; Torres-Vázquez et al., 2004; Zhang et al., 2009). Sema3E activates PlexinD1 independently of Nrp, which triggers actin depolymerization and cellular collapse by reducing Rac1 activity through the RhoGAP domain of SH3BP1 (Tata et al., 2014). The Sema3E/PlexinD1 axis counteracts VEGF-induced filopodial projections at the front of actively sprouting blood vessels, indicating that PlexinD1 provides a repulsive guidance cue in endothelial cells (Fukushima et al., 2011; Kim et al., 2011). However, it remains to be elucidated whether PlexinD1 plays a role in lymphatic vascular patterning.

Sema3G is the most recently discovered member of class 3 semaphorins. Growing evidence implicates Sema3G in cell migration and axon guidance (Bron et al., 2007; Karayan-Tapon et al., 2008). Previous studies showed that Sema3G strongly binds to Nrp2 and induces repulsion of sympathetic axons or migration of smooth muscle cells (SMCs) in culture, but little is known about its signaling mechanisms (Kutschera et al., 2011; Taniguchi et al., 2005). Furthermore, previous studies in mice revealed a preferential expression pattern in developing arterial endothelial cells, but they did not detect any overt vascular phenotype in Sema3G-deficient mice (Kutschera et al., 2011; Uchida et al., 2015). Thus, to date, the in vivo role of Sema3G in vascular development remains unclear.

In this study, we investigated lymphatic vascular development in PlexinD1- or Sema3G-deficient mouse embryos and found that these molecules are important for LECs to be repelled from arteries in mouse embryonic skin. We also performed in vitro analyses demonstrating that Sema3G activates PlexinD1 through the binding of Nrp2. Here, we show that Sema3G provides a repulsive guidance cue from arteries to PlexinD1$^+$ LECs during lymphatic vascular patterning.

RESULTS

Lymphatic Vascular Formation Is Initiated Near Large-Caliber Blood Vessels and Eventually Extends Away from Them in Mouse Embryonic Back Skin

We and others previously reported that embryonic back skin is a good model for studying lymphatic vascular patterning in mice (Hirashima et al., 2008; James et al., 2013; Martinez-Corral et al., 2015). To investigate lymphatic vascular pattering as well as blood vessel development in the thoracic region of embryonic back skin, we performed whole-mount triple-fluorescence confocal microscopy using antibodies to the pan-endothelial marker PECAM-1, α-smooth muscle actin (αSMA), and the LEC marker Nrp2 (Yuan et al., 2002). At embryonic day 12.5 (E12.5), a portion of the blood vessel becomes enlarged, suggesting it is undergoing a process of blood vessel remodeling. However, no part of the vasculature is covered by SMCs (data not shown), and only a small number of LECs are first detected in this region (Figure S1). By E13.5, large-caliber blood vessels are formed and partly covered by SMCs. An incomplete lymphatic network with filopodial extensions for subsequent branching sites is formed near large-caliber blood vessels. LECs are especially associated with αSMA$^+$ blood vessels, suggesting that lymphatic vascular development follows blood vessel remodeling in mouse embryonic back skin (Figures 1A–1C). After E14.5, blood vessels are further remodeled to acquire coverage by SMCs, and a more widely distributed lymphatic network is detected (Figures 1D–1F). At E15.5, lymphatic vessels appear less associated with large-caliber blood vessels than those at earlier stages in the thoracic region of embryonic back skin (Figures 1G–1I). These results suggest that lymphatic network formation in mouse embryonic back skin is tightly regulated by some guidance cues from blood vessels.

PlexinD1$^{-/-}$ Embryos Show Abnormal Artery-Lymph Alignment and Defective Venous Formation in Mouse Embryonic Back Skin

Given that PlexinD1 signaling has been implicated in a repulsive guidance cue during blood vascular network formation (Carmeliet and Tessier-Lavigne, 2005; Eichmann et al., 2005; Kim et al., 2011), we studied the role of PlexinD1 in lymphatic vascular patterning of mouse embryonic back skin. We first characterized the expression of PlexinD1 by immunohistochemistry of whole-mount or transverse sections of mouse embryonic back skin using antibodies to PlexinD1 and the LEC marker Lyve-1. This analysis detected PlexinD1 expression in Lyve-1$^+$ LECs as well as BECs (Figures S2A–S2F). RT-PCR analysis also detected *PlexinD1* expression in LECs purified from mouse embryonic back skin (Figure S2G). We investigated the network formation of blood and lymphatic vessels in *PlexinD1*$^{-/-}$ embryonic back skin by whole-mount double fluorescence confocal microscopy using antibodies to PECAM-1 and the LEC marker VEGFR3 at E15.5. Lymphatic vessels form a random network whose pattern is not related to blood vessels in control littermates, whereas lymphatic vessels are tightly associated with large-caliber blood vessels in both the proximal lymphatic network and the distal migration front of *PlexinD1*$^{-/-}$ embryos, leading to reduced lymphatic vascular branching (Figures 2A–2H, 2M, and 2N). To investigate blood vessels in more detail, we used antibodies to the arterial endothelial marker connexin 40 (Cx40) and VEGFR3 for confocal microscopy of embryonic back skin at E15.5. This analysis identified arteries as the large-caliber blood vessels associated with VEGFR3$^+$ lymphatic vessels in *PlexinD1*$^{-/-}$ embryos (Figures S2H and S2I). We further measured the number of Prox1$^+$ LECs, but there was no significant difference between *PlexinD1*$^{+/-}$ and *PlexinD1*$^{-/-}$ embryos (Figure S2J), suggesting that abnormal lymphatic patterning is caused by the abnormal distribution of LECs in *PlexinD1*$^{-/-}$ embryos. We also noticed that MECA32 antibody predominantly detects venous and capillary endothelial cells in the embryonic back skin of control littermates, but the formation of large-caliber veins is disturbed in *PlexinD1*$^{-/-}$ embryos (Figures 2I–2L and 2O).

Conditional Ablation of PlexinD1 in LECs Results in Abnormal Artery-Lymph Alignment, but Not a Defect in Venous Formation, in Mouse Embryonic Back Skin

PlexinD1$^{-/-}$ embryos show defects in both venous and lymphatic vessel formation, raising the possibility that lymphatic

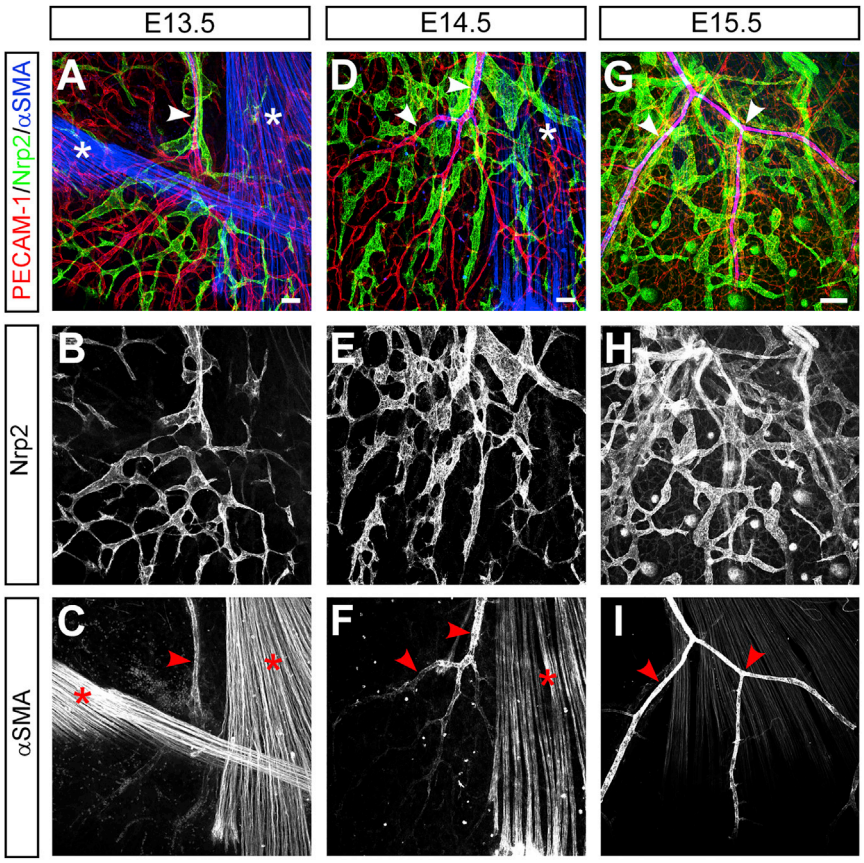

Figure 1. Lymphatic Vascular Formation Is Spatially Related to Large-Caliber Blood Vessels in Mouse Embryonic Back Skin

Whole-mount immunohistochemistry of mouse embryos at E13.5 (A–C) and back skin at E14.5 (D–F) or E15.5 (G–I) is shown for PECAM-1 (A, D, and G, red), Nrp2 (A, D, and G, green; B, E, and H, white), and α-SMA (A, D, and G, blue; C, F, and I, white). In mouse embryonic back skin, large-caliber blood vessels are formed and covered partly by SMCs (arrowheads), and initial lymphatic vessel network is seen near the developing large-caliber blood vessels at E13.5. Blood vessels further remodel to acquire coverage by SMCs and a more widely distributed lymphatic network is seen after E14.5. Asterisks indicate skeletal muscles. Scale bars, 100 μm. See also Figure S1.

vessels may have replaced a space adjacent to arteries owing to the lack of veins. To address whether PlexinD1 is primarily important in LECs, we decided to ablate PlexinD1 using a *Prox1*$^{GFPCre/+}$ LEC-specific Cre deleter mouse strain. To confirm the specificity of Cre activity in LECs, *Prox1*$^{GFPCre/+}$ mice were crossed with the *Rosa26*$^{floxed\text{-}lacZ/+}$ Cre reporter mouse strain. X-gal staining followed by triple-fluorescence immunohistochemistry of *Prox1*$^{GFPCre/+}$; *Rosa26*$^{floxed\text{-}lacZ/+}$ embryonic back skin using antibodies to VEGFR3, the neurofilament marker 2H3, and PECAM-1 at E15.5 showed that the lacZ reporter is detected specifically in lymphatic vessels, but not in neurons or blood vessels (Figures S3A–S3D). LEC-specific PlexinD1 conditional knockout *Prox1*$^{GFPCre/+}$; *PlexinD1*$^{flox/-}$ (*PlexinD1*$^{\Delta LEC}$) mice were generated by mating *Prox1*$^{GFPCre/+}$; *PlexinD1*$^{+/-}$ mice and *PlexinD1*$^{flox/flox}$ mice. Confocal microscopy of *PlexinD1*$^{\Delta LEC}$ embryonic back skin using antibodies to PlexinD1, Lyve-1, 2H3, and PECAM-1 at E15.5 confirmed that PlexinD1 expression is lost specifically in lymphatic vessels but is still present in neurons and blood vessels (Figures S3E–S3I). Since the *Prox1*$^{GFPCre/+}$ strain is haploinsufficient for the *Prox1* gene and itself shows developmental abnormalities (Srinivasan et al., 2007), *Prox1*$^{GFPCre/+}$; *PlexinD1*$^{flox/+}$ mice were exclusively analyzed as control littermates. We performed whole-mount double-fluorescence confocal microscopy of embryonic back skin using antibodies to Cx40 and VEGFR3 at E15.5. *PlexinD1*$^{\Delta LEC}$ embryos showed an abnormal artery-lymph alignment similar to that in conventional PlexinD1 knockout embryos. Lymphatic vessels are tightly associated with large-caliber blood vessels in both the proximal lymphatic network and distal migration front, leading to reduced lymphatic vascular branching (Figure 3A–3H, 3M, and 3N). On the other hand, confocal microscopy of embryonic back skin using antibodies to Cx40 and MECA32 confirmed that the formation of large-caliber veins adjacent to arteries is not affected in *PlexinD1*$^{\Delta LEC}$ embryos at E15.5 (Figure 3I–3L and 3O). These results indicate that abnormal artery-lymph alignment is caused primarily by the loss of PlexinD1 in LECs.

Sema3G$^{lacZ/lacZ}$ Embryos Show Abnormal Artery-Lymph Alignment and Defective Venous Formation in Mouse Embryonic Back Skin

We next tried to identify the PlexinD1 ligand responsible for proper lymphatic vascular patterning in mouse embryonic back skin. Since it has been reported that Sema3E, the ligand for PlexinD1, is implicated in a repulsive guidance cue in endothelial cells (Fukushima et al., 2011; Kim et al., 2011), we investigated the network formation of blood and lymphatic vessels in *Sema3E*$^{-/-}$ embryos. We performed whole-mount double-fluorescence confocal microscopy of embryonic back skin using antibodies to PECAM-1 and VEGFR3 at E15.5. Analysis of *Sema3E*$^{-/-}$ embryos showed that lymphatic vessels form a random network with a pattern that is not related to blood vessels (Figure S4), indicating that Sema3E is not required for proper lymphatic vascular patterning in mouse embryonic back skin.

Previous studies reported that Sema3G is preferentially expressed in arterial endothelial cells, but Sema3G-deficient mice exhibit no overt vascular phenotype (Kutschera et al., 2011; Uchida et al., 2015). We also investigated the expression pattern of Sema3G by using a different *Sema3G*^{lacZ} mouse strain carrying a lacZ reporter in the *Sema3G* locus and confirmed the preferential expression in arteries by X-gal staining of

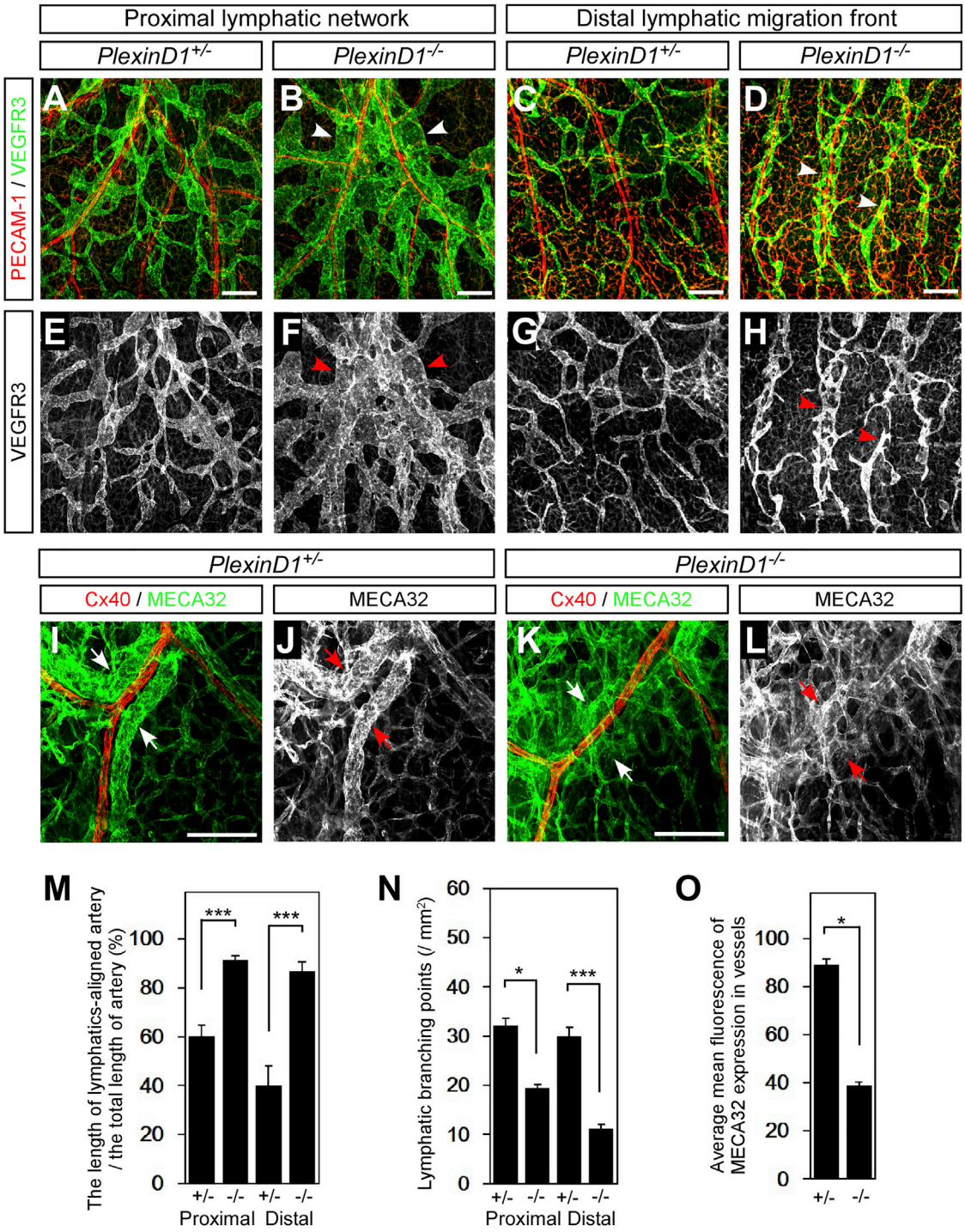

Figure 2. *PlexinD1*$^{-/-}$ Embryos Show Abnormal Artery-Lymph Alignment and Defective Venous Formation in Mouse Embryonic Back Skin

Whole-mount immunohistochemistry of back skin is shown for PECAM-1 (A–D, red), VEGFR3 (A–D, green; E–H, white), Cx40 (I and K, red), and MECA32 (I and K, green; J and L, white) at E15.5. Lymphatic vessels are more tightly associated with large-caliber blood vessels in both the proximal lymphatic network and distal migration front in *PlexinD1*$^{-/-}$ embryos (arrowheads) compared with control littermates. Formation of the venous structure is disturbed in *PlexinD1*$^{-/-}$ embryos compared with control littermates (arrows). Scale bars, 100 μm. Statistical analyses of artery-lymph arrangement (M, n = 5 each group), lymphatic branching (N, n = 5 each group), and venous formation (O, n = 3 each group). Values are presented as mean ± SEM. ***$p < 0.001$, *$p < 0.05$, unpaired two-tailed Student's t test. See also Figures S2 and S7.

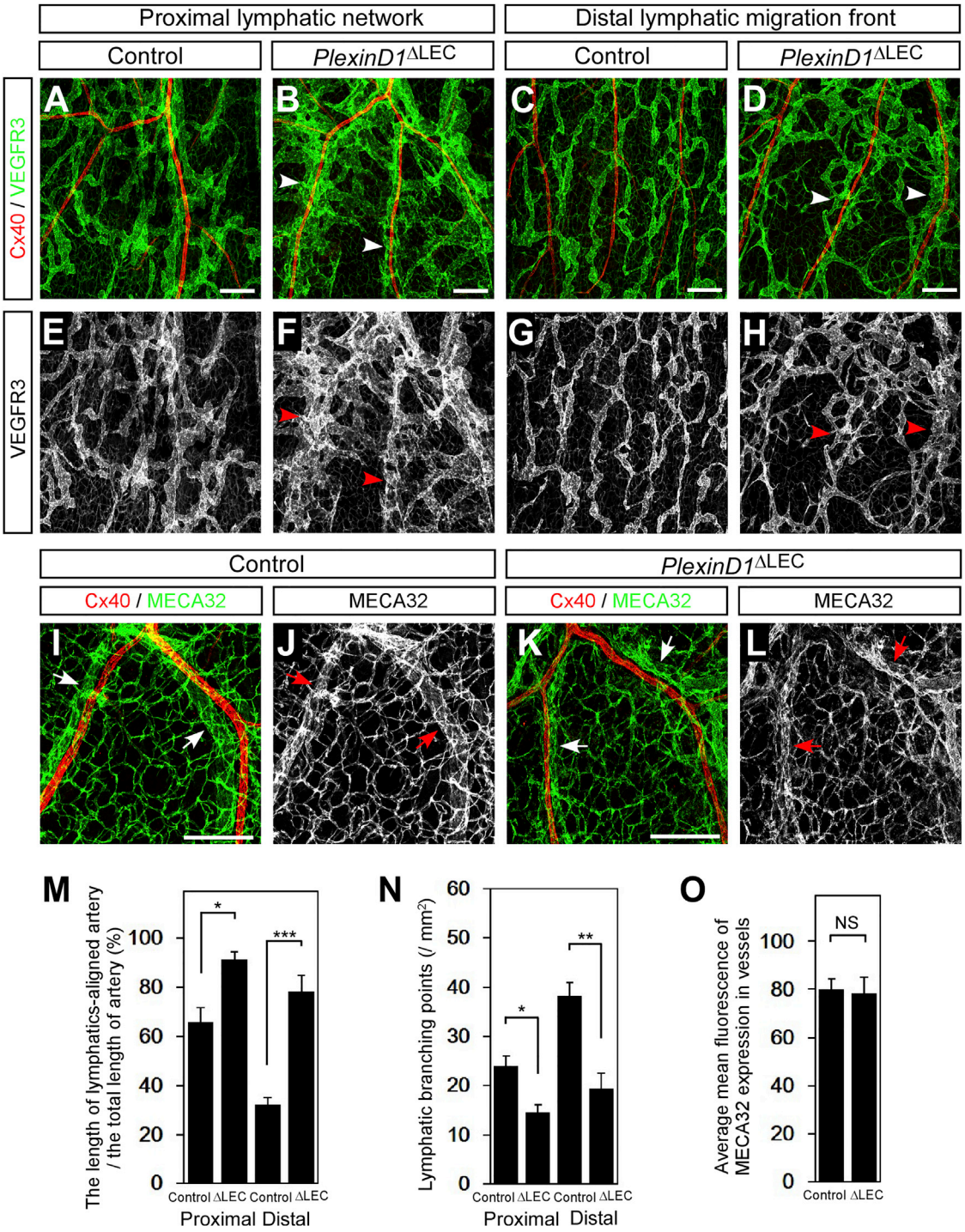

Figure 3. Loss of PlexinD1 in LECs Results in Abnormal Artery-Lymph Alignment but Normal Venous Formation in Mouse Embryonic Back Skin

Whole-mount immunohistochemistry of back skin is shown for Cx40 (A–D, I, and K, red), VEGFR3 (A–D, green; E–H, white), and MECA32 (I and K, green; J and L, white) at E15.5. In *PlexinD1*$^{\Delta LEC}$ embryos, lymphatic vessels are more tightly associated with large-caliber blood vessels in both the proximal lymphatic network and distal migration front (arrowheads) compared with control littermates. Formation of the venous structure is normal compared with control littermates (arrows). Scale bars, 100 μm. Statistical analyses of artery-lymph arrangement (M, n = 3 each group), lymphatic branching (N, n = 3 each group), and venous formation (O, n = 3 each group). Values are presented as mean ± SEM. ***$p < 0.001$, **$p < 0.01$, and *$p < 0.05$; NS, not significant, unpaired two-tailed Student's t test. See also Figures S3 and S7.

Sema3G$^{+/lacZ}$ embryonic back skin at E15.5 (Figures S5A–S5C). We thus hypothesized that Sema3G is a good candidate for the ligand, serving as a repulsive guidance cue from arteries to LECs that appears to be defective in *PlexinD1*$^{-/-}$ or *PlexinD1*$^{\Delta LEC}$ embryos. To investigate whether Sema3G contributes to proper lymphatic vascular patterning in mouse embryonic back skin, we performed whole-mount double-fluorescence confocal microscopy using antibodies to PECAM-1 and VEGFR3 at E15.5. *Sema3G*$^{lacZ/lacZ}$ embryos showed abnormal artery-lymph alignment similar to that in *PlexinD1*$^{-/-}$ or *PlexinD1*$^{\Delta LEC}$ embryos. Lymphatic vessels are tightly associated with large-caliber blood vessels in both the proximal lymphatic network and distal migration front, leading to reduced lymphatic vascular branching (Figure 4A–4H, 4M, and 4N). Moreover, confocal microscopy of embryonic back skin using antibodies to Cx40, VEGFR3, and MECA32 showed that the large-caliber blood vessels associated with lymphatic vessels are arteries (Figure S5D and S5E, arrowheads) and the formation of large-caliber veins is disturbed in *Sema3G*$^{lacZ/lacZ}$ embryos at E15.5 (Figures 4I–4L and 4O). However, these abnormalities in artery-lymph alignment and venous formation appear transient in *Sema3G*$^{lacZ/lacZ}$ mice, since they are not detected at E17.5 (Figures S5F–S5J, arrows) or in the adult ear skin (data not shown). These results indicate that vascular defects in the back skin of *Sema3G*$^{lacZ/lacZ}$ embryos are very similar to those found in *PlexinD1*$^{-/-}$ embryos.

Sema3G Binds to a Receptor Complex Composed of Nrp2 and PlexinD1

Given the similarity of lymphatic vascular phenotypes between *PlexinD1*$^{-/-}$ and *Sema3G*$^{lacZ/lacZ}$ embryos, we hypothesized that Sema3G may provide signals to LECs through PlexinD1. Previous reports showed that Sema3G binds to Nrp2 (Kutschera et al., 2011; Taniguchi et al., 2005), but the interaction between Sema3G and PlexinD1 remains to be elucidated. To investigate whether Sema3G binds to PlexinD1 as well as Nrp2, COS-7 cells were transfected with expression vectors carrying PlexinD1, Nrp2 fused to FLAG tag (Nrp2-FLAG), or both. The transfected cells were incubated with Sema3G fused to alkaline phosphatase (Sema3G-AP) or Sema3E-AP as a control and stained for alkaline phosphatase (AP) activity to detect the ligand binding. Consistent with a previous finding (Gu et al., 2005), we found that Sema3E-AP directly binds to PlexinD1-expressing cells (Figure 5B and 5D), whereas Sema3G-AP binds to Nrp2-expressing cells (Figures 5G and 5H). On the other hand, Sema3G-AP did not bind to PlexinD1-expressing cells in the absence of Nrp2 (Figure 5F), indicating that PlexinD1 is not a direct receptor for Sema3G. We next investigated the possibility that Nrp2 works as a co-receptor with PlexinD1. HEK293T cells were transfected with expression vectors carrying PlexinD1, Nrp2-FLAG, or both, followed by co-immunoprecipitation experiments. Western blot analysis following immunoprecipitation of cell lysates with an antibody to FLAG detected the presence of PlexinD1 protein mostly when cells were transfected only with both Nrp2-FLAG and PlexinD1 (Figure 5I). To confirm the binding between Nrp2 and PlexinD1 endogenous proteins, we used human dermal lymphatic microvascular endothelial cells (HMVEC-dLyNeo) for co-immunoprecipitation experiment, since these two proteins were detected by western blot (Figure 5J, input). Western blot analysis following immunoprecipitation of HMVEC-dLyNeo lysates with an antibody to Nrp2 actually detected the presence of PlexinD1 protein (Figure 5J), indicating that Nrp2 and PlexinD1 bind to each other to form a receptor complex in LECs.

Sema3G Induces Cell Collapse in an Nrp2/PlexinD1-Dependent Manner and Exhibits a Repulsive Activity to Primary LECs

In a binding analysis, we noticed that Sema3E-AP induces cell collapse of PlexinD1-expressing cells (Figure 5B, arrows), as reported previously (Gu et al., 2005). Similarly, we noticed that Sema3G-AP induces cell collapse of some AP-positive cells, but only when COS-7 cells were transfected with both PlexinD1 and Nrp2 (Figure 5H, arrows). We thus investigated whether Sema3G induces cell collapse in an Nrp2/PlexinD1-dependent manner. COS-7 cells were transfected with expression vectors carrying PlexinD1, Nrp2-FLAG, or both, followed by treatment with Sema3G-AP protein. The expression of PlexinD1 and Nrp2-FLAG proteins was checked by immunocytochemistry using antibodies to PlexinD1, Nrp2, and FLAG together with phalloidin, a marker for F-actin. Without Sema3G-AP treatment, cell size is comparable among cells after transfection (Figure S6). Sema3G-AP does not induce cell collapse of cells expressing either PlexinD1 (Figures 6B and 6C) or Nrp2 (Figures 5G and 6D–6F) alone. When COS-7 cells were transfected with both and treated with Sema3G-AP, cell collapse was observed only in cells expressing both PlexinD1 and Nrp2 proteins (Figures 6G–6J, arrows), indicating that Sema3G works in an Nrp2/PlexinD1-dependent manner. To investigate whether Sema3G affects LEC migration induced by VEGF-C, we performed wound-healing and transwell migration assays using HMVEC-dLyNeo cells. Sema3G did not affect VEGF-C-induced migration (Figure 6K), whereas Sema3G added to the lower chamber suppressed VEGF-C-induced transwell migration from the upper to lower surface of a cell-permeable membrane (Figure 6L). These results indicate that Sema3G does not affect LEC motility but serves as a repulsive factor for LECs.

DISCUSSION

In this study, we found that proper patterning of LECs is regulated by the Sema/Plexin signaling pathway mediated by the artery-derived ligand Sema3G and the LEC receptors Nrp2 and PlexinD1 (Figure 7). Genetic inactivation of Sema3G or PlexinD1 results in abnormal artery-lymph alignment and reduces lymphatic vascular branching in mouse embryonic back skin. In vitro analyses showed that Sema3G binds to the Nrp2/PlexinD1 receptor complex, induces cell collapse, and exhibits a repulsive effect on primary LECs. Our findings shed light on a mechanism by which LECs can be distributed away from arteries and form a branching network during lymphatic vascular development.

PlexinD1 Signals in LECs Regulate Lymphatic Vascular Patterning in Mouse Embryonic Back Skin

In the zebrafish trunk, arteries provide essential guidance cues for LECs (Bussmann et al., 2010). Our results using mouse

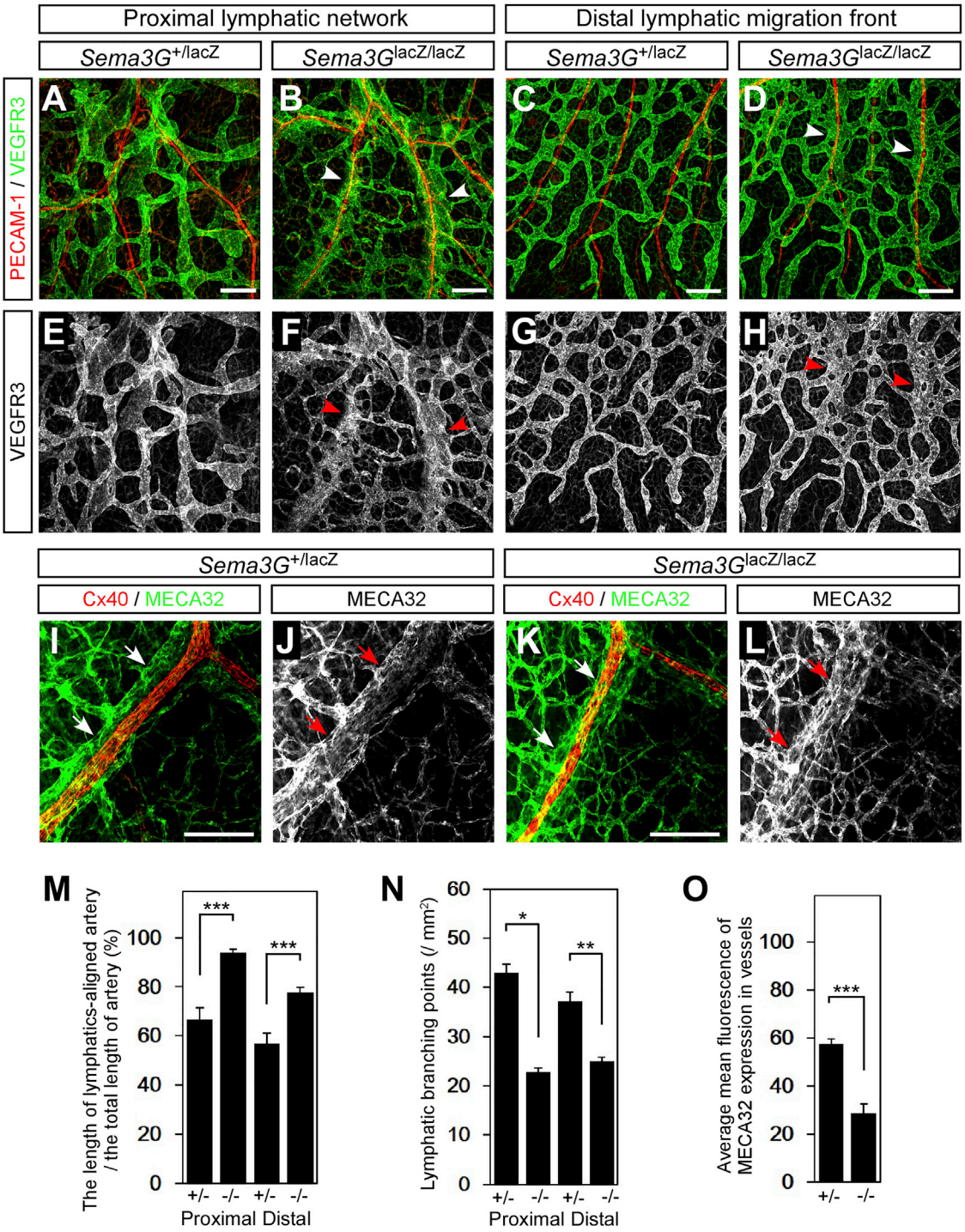

Figure 4. *Sema3G*$^{lacZ/lacZ}$ Embryos Show Abnormal Artery-Lymph Alignment and Defective Venous Formation in Mouse Embryonic Back Skin

Whole-mount immunohistochemistry of back skin is shown for PECAM-1 (A–D, red), VEGFR3 (A–D, green; E–H, white), Cx40 (I and K, red), and MECA32 (I and K, green; J and L, white) at E15.5. Lymphatic vessels are more tightly associated with large-caliber blood vessels in both the proximal lymphatic network and distal migration front in *Sema3G*$^{lacZ/lacZ}$ embryos (arrowheads) compared with control littermates. Formation of the venous structure is disturbed in *Sema3G*$^{lacZ/lacZ}$ embryos compared with control littermates (arrows). Scale bars, 100 μm. Statistical analyses of artery-lymph arrangement (M, *Sema3G*$^{+/lacZ}$, n = 4, *Sema3G*$^{lacZ/lacZ}$, n = 9), lymphatic branching (N, *Sema3G*$^{+/lacZ}$, n = 4, *Sema3G*$^{lacZ/lacZ}$, n = 9), and venous formation (O, n = 3 each group). Values are presented as mean ± SEM. ***$p < 0.001$, **$p < 0.01$, *$p < 0.05$, unpaired two-tailed Student's t test. See also Figures S4, S5, and S7.

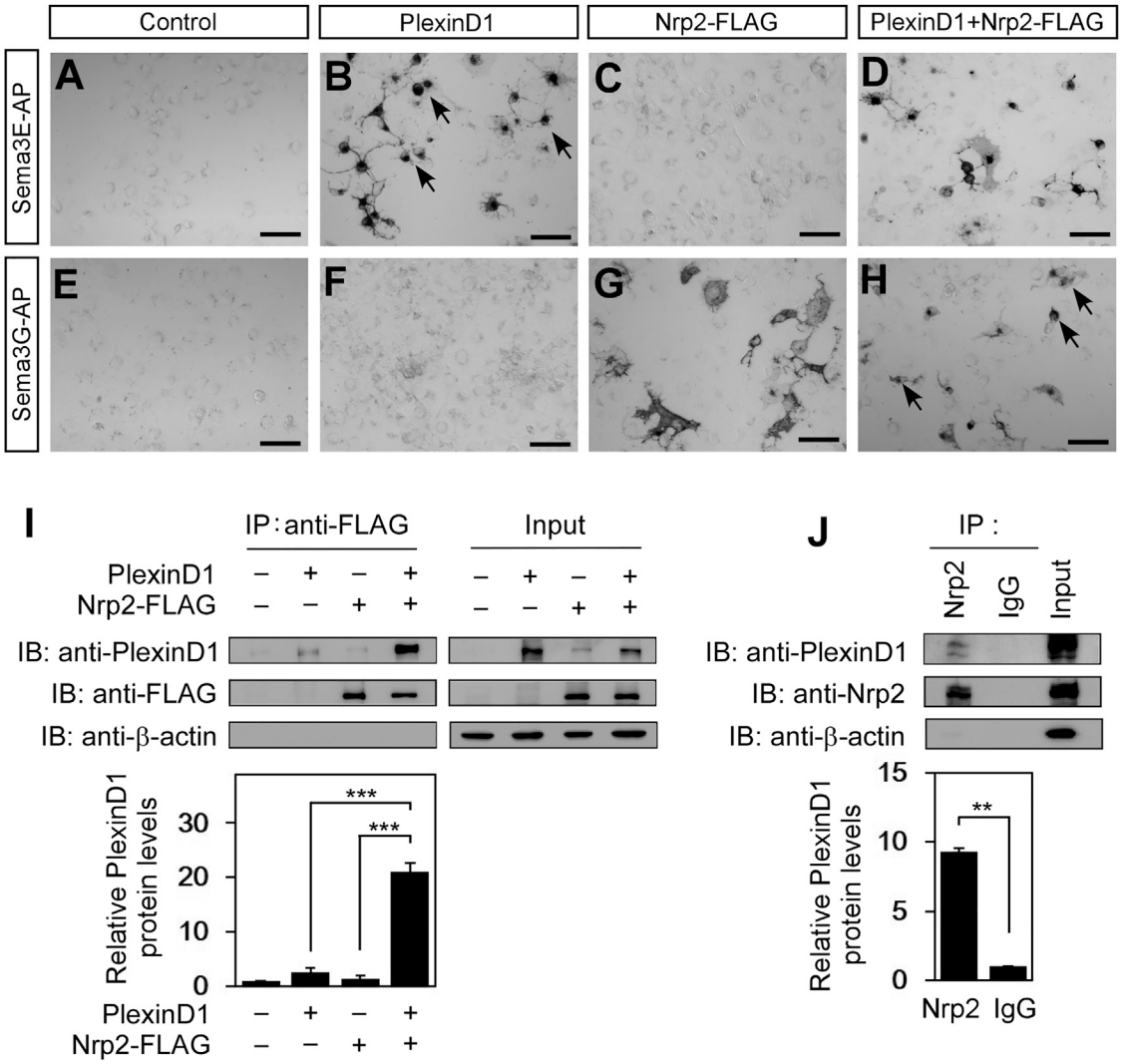

Figure 5. Sema3G Binds to the Nrp2/PlexinD1 Complex

(A–H) AP-stained COS-7 cells are shown after being transfected with expression vectors carrying PlexinD1 (B and F), Nrp2-FLAG (C, G), or both (D and H) and incubated with supernatants containing Sema3E-AP or Sema3G-AP. Sema3E-AP, but not Sema3G-AP, directly binds to PlexinD1-expressing cells, whereas Sema3G-AP, but not Sema3E-AP, binds to Nrp2-expressing cells. Scale bars, 100 μm.

(I) Western blot following immunoprecipitation experiments. HEK293T cells were transfected with expression vectors carrying PlexinD1, Nrp2-FLAG, or both. Lysates were immunoprecipitated using anti-FLAG antibody. The immunoprecipitates were probed using anti-PlexinD1, anti-FLAG, and anti-β-actin antibodies. The value from the experiment without vectors was arbitrarily set at 1 (n = 5 each group). ***$p < 0.001$, one-way ANOVA followed by Tukey-Kramer test for multiple comparisons.

(J) Western blot following immunoprecipitation experiments. Lysates from HMVEC-dLyNeo cells were immunoprecipitated using control (immunoglobulin G [IgG]) or anti-Nrp2 antibody. The immunoprecipitates were probed using anti-PlexinD1, anti-Nrp2, and anti-β-actin antibodies. The value from the control experiment was arbitrarily set at 1 (n = 5 each group).

Values are presented as mean ± SEM. **$p < 0.01$; NS, not significant, unpaired two-tailed Student's t test.

embryonic back skin also show that LECs are distributed near arteries at an early stage, suggesting that arteries provide attractive guidance cues, such as soluble factors and/or extracellular matrix for the migration of LEC precursors (François et al., 2012). A previous study in zebrafish embryos identified Cxcl12 released from arterial endothelial cells as an attractive guidance cue (Cha et al., 2012). In mouse embryonic back skin, the distribution of LEC precursors near arteries appears to be related to SMC investment, suggesting an involvement of SMC-derived factors such as VEGF-C (Nurmi et al., 2015).

During the following stages, LECs are distributed into vacant areas and form a lymphatic capillary network. We found abnormal artery-lymph alignment and reduced lymphatic vascular branching in the back skin of *PlexinD1*$^{-/-}$ embryos. These two phenotypes appear to be closely associated with each other, since both are affected by LEC distribution patterns

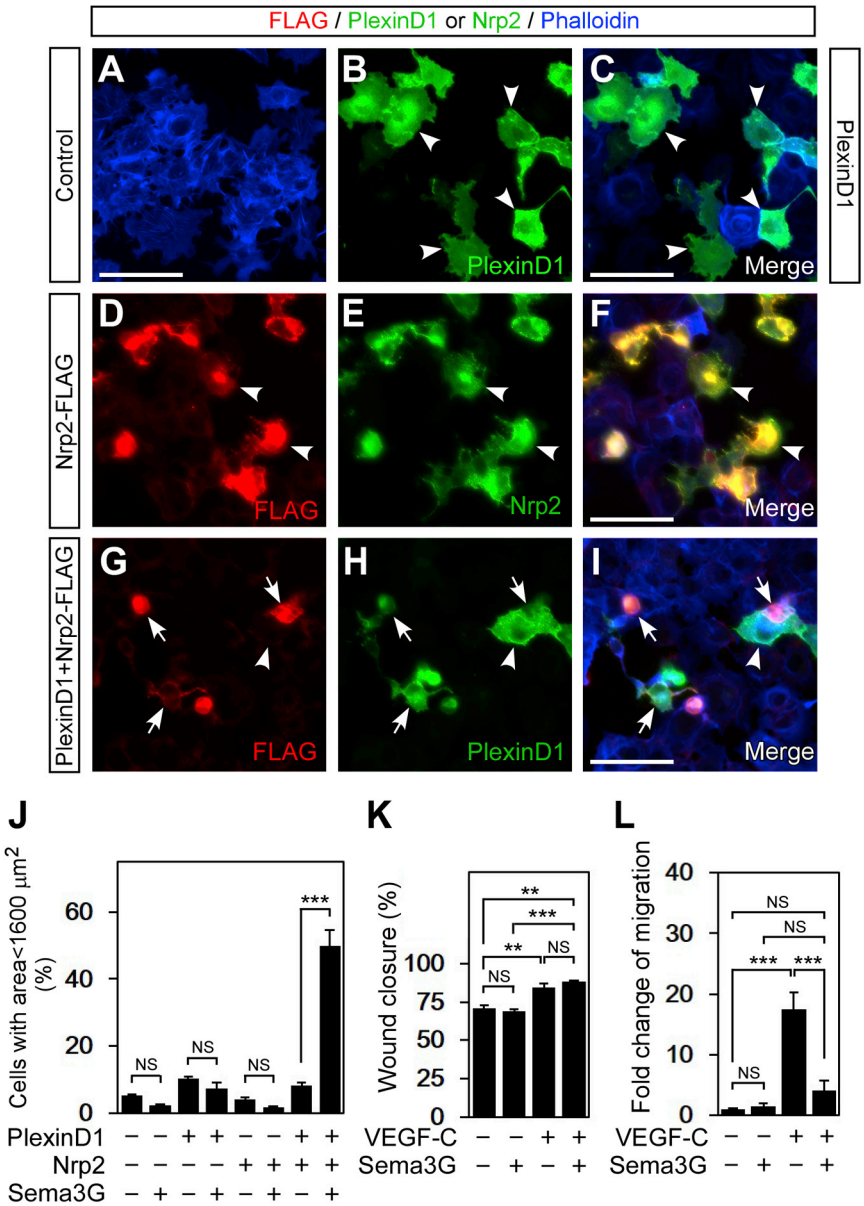

Figure 6. Sema3G Induces Cell Collapse in an Nrp2/PlexinD1-Dependent Manner and Exhibits a Repulsive Effect on Primary LECs

(A–I) Immunocytochemistry of COS-7 cells is shown after being transfected with expression vectors carrying PlexinD1 (B and C), Nrp2-FLAG (D–F), or both (G–I), incubated with supernatants containing Sema3G-AP, and stained by using antibodies to PlexinD1 (B, C, H, and I, green), FLAG (D, F, G, and I, red), Nrp2 (E and F, green), and phalloidin (A, C, F, and I, blue). Note that cell collapse induced by Sema3G-AP is observed in cells expressing both PlexinD1 and Nrp2-FLAG proteins (G–I, arrows), but not in those expressing either PlexinD1 (B, C, and G–I, arrowheads) or Nrp2-FLAG alone (D–F, arrowheads). Scale bars, 100 μm.

(J) Statistical analysis of the percentage of collapsed cells with area less than 1,600 μm^2 (n = 3 each group).

(K) Migration of HMVEC-dLyNeo cells in the presence of VEGF-C and/or Sema3G was measured as a percentage of wound closure after 24 hr (n = 3 each group).

(L) Transwell migration of HMVEC-dLyNeo cells placed on the upper surface of a cell-permeable membrane was evaluated in the presence of VEGF-C and/or Sema3G in the lower chamber. Relative cell migration was determined by the number of migrated cells. The value from the experiment without factors was arbitrarily set at 1 (n = 3 each group).

Values are presented as mean ± SEM. ***$p < 0.001$, **$p < 0.01$; NS, not significant, one-way ANOVA followed by Tukey-Kramer test for multiple comparisons. See also Figure S6.

without a change in LEC number. In other words, when more LECs are distributed near arteries, fewer LECs can contribute to branching network formation. Despite the proximity between lymphatic vessels and blood vessels, abnormal lymph-blood mixing or shunt between the two vascular compartments is not detected in *PlexinD1*$^{-/-}$ embryos, indicating that PlexinD1 signals are dispensable for proper separation of lymphatic and blood vasculature.

PlexinD1 is expressed in the vascular endothelium and CNS (Gitler et al., 2004; Gu et al., 2005). Previous studies detected multiple cardiovascular defects in *PlexinD1*$^{-/-}$ mice, including atrial enlargement, outflow tract defect, coronary artery anomaly, and disorganized intersomitic vessels (Gitler et al., 2004; Zhang et al., 2009). A variety of studies in mice have also implicated PlexinD1 in various aspects of nervous system development (Bellon et al., 2010; Chauvet et al., 2007). Since arterial development in the embryonic skin is also influenced by nerve-provided cues (Mukouyama et al., 2002), abnormal association between arteries and lymphatic vessels might be secondary to these other cardiovascular or nervous defects in *PlexinD1*$^{-/-}$ mice. However, our conditional knockout analysis of *PlexinD1*$^{\Delta LEC}$ embryos demonstrated that PlexinD1 expression in LECs is responsible for proper lymphatic vascular patterning to inhibit abnormal artery-lymph alignment. This is consistent with previous reports showing that PlexinD1 signals serve as a repulsive guidance cue in blood vessel formation during embryogenesis or in the oxygen-induced retinopathy model (Fukushima et al., 2011; Gu et al., 2005; Kim et al., 2011). On the other hand, the role of lymphatic PlexinD1 in adulthood remains to be elucidated owing to perinatal lethality of *PlexinD1*$^{-/-}$ mice or *PlexinD1*$^{\Delta LEC}$ mice carrying *Prox1*^{GFPCre} haploinsufficient mutation (Gu et al., 2005; Srinivasan et al., 2007). Our results indicate that LECs receive a repulsive guidance cue from arteries through PlexinD1 to form a random lymphatic vascular network in mouse embryonic back skin.

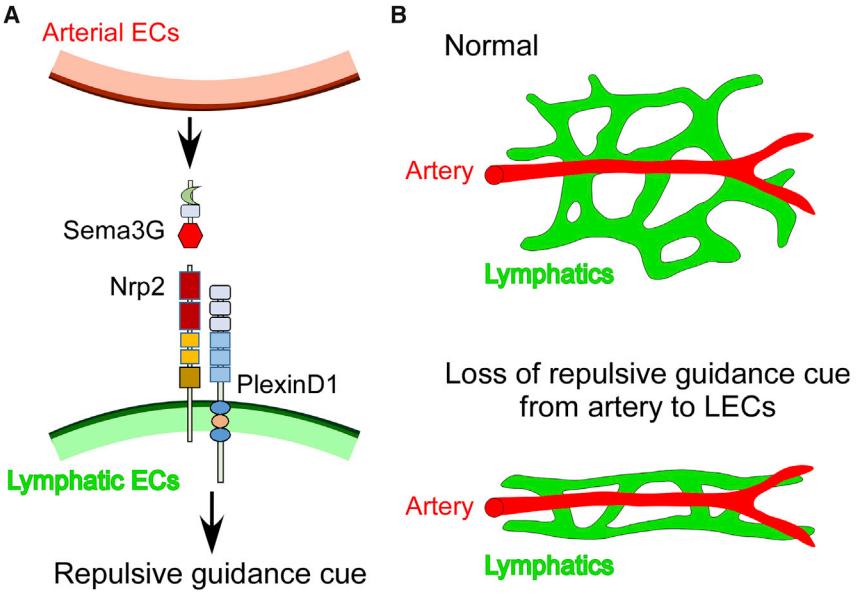

Figure 7. Arterial Sema3G Provides a Repulsive Guidance Cue to PlexinD1$^+$ LECs

(A) Sema3G protein released by arterial endothelial cells binds to the Nrp2/PlexinD1complex on LECs, which plays a role in the repulsion of LECs away from arteries.

(B) Loss of Sema3G or PlexinD1 results in abnormal artery-lymph alignment and reduced lymphatic vascular branching in mouse embryonic back skin.

Sema3G Is the Ligand for PlexinD1-Mediated Lymphatic Vascular Network Formation

To our surprise, Sema3E, a direct ligand for PlexinD1, is dispensable for proper lymphatic vascular patterning in mouse embryonic back skin, while it has been reported to regulate blood vessel patterning (Gu et al., 2005). On the other hand, we found that mice deficient in an artery-specific ligand, Sema3G, show abnormal artery-lymph alignment and reduced lymphatic vascular branching without lymph-blood mixing in the embryonic back skin, which is also seen in *PlexinD1*$^{-/-}$ mice. Migration assays showed that Sema3G does not inhibit VEGF-C-induced migration but exhibits a repulsive effect on primary LECs. These results suggest that Sema3G is a repulsive guidance cue from arteries to PlexinD1$^+$ LECs. Although Sema3G does not bind directly to PlexinD1, co-immunoprecipitation analysis using transfected cells and primary LECs indeed showed that Nrp2, a receptor for Sema3G, binds to PlexinD1. More importantly, Sema3G selectively induces the collapse of PlexinD1$^+$ cells when Nrp2 protein is co-expressed. Although it has been proposed that Sema3G binds to Nrp2 in a complex with PlexinA family proteins (Gaur et al., 2009), our result is the demonstration that Sema3G induces PlexinD1-mediated cellular responses. This Nrp2-dependent PlexinD1 signaling mechanism for Sema3G in LECs is very similar to previous findings regarding other Sema/Nrp/Plexin family members. Sema3A and Sema3F have a repellent effect on endothelial cells in an Nrp1- or Nrp2-dependent manner, respectively (Guttmann-Raviv et al., 2007). Sema3A/Nrp1/PlexinA1 signals have been implicated in cell repulsion during lymphatic valve formation (Bouvrée et al., 2012; Jurisic et al., 2012).

A previous study reported that Nrp2 is required for lymphatic vascular development in mice (Yuan et al., 2002), and we detected the enlargement of lymphatic vessels, but not abnormal artery-lymph alignment, in the back skin of *Nrp2*$^{-/-}$ mouse embryos (data not shown). The discrepancy in lymphatic phenotype between Sema3G/PlexinD1- and Nrp2-deficient mouse embryos is probably related to the fact that Nrp2 is a co-receptor for VEGF-C and also interacts with other signaling pathways, such as transforming growth factor β (TGF-β), hepatocyte growth factor (HGF), or integrin signaling (Grandclement et al., 2011; Ou et al., 2015; Sulpice et al., 2008; Xu et al., 2010). Since the VEGF-C/VEGFR3 axis plays a critical role in lymphatic vessel formation, loss of Nrp2 results in lymphatic sprouting defects caused by a change in VEGF-C signals. Moreover, Nrp2 binds to several members of the class 3 semaphorin family, including Sema3B, 3C, 3F, and 3G (Neufeld and Kessler, 2008). Sema3C induces glomerular endothelial cell proliferation and elicits a repulsive guidance cue through Nrp2 (Banu et al., 2006; Ruediger et al., 2013). Sema3F functions as a repellent cue of LECs in tumors (Bielenberg et al., 2004). Since Nrp2 interacts with many proteins that have been implicated in cellular migratory and cell extension behaviors, the in vivo role of Nrp2 in lymphatic vascular patterning remains to be elucidated.

We analyzed lymphatic vessels in embryonic mesenteries, but abnormal artery-lymph alignment was not detected in *Sema3G* or *PlexinD1* knockout embryos (data not shown). Origins of LECs are different among organs (Martinez-Corral et al., 2015; Stanczuk et al., 2015), and Sema3G might play a different role in the incorporation of non-venous-derived cells into the growing lymphatic vasculature. We so far detected the abnormal phenotype of artery-lymph alignment only in the embryonic back skin of *Sema3G*$^{lacZ/lacZ}$ mice, suggesting a compensatory mechanism such as another set of repulsive cues at later stages. Alternatively, the repulsive signal from arterial endothelial cells (ECs) might play a role predominantly at earlier stages, when the immature arterial SMC layer allows diffusion of Sema3G, which is more accessible to LECs. Further experiments will be required to address these possibilities of spatiotemporally restricted involvement of Sema3G in lymphatic vascular patterning. In conclusion, our study clearly shows that arterial Sema3G and lymphatic PlexinD1 play a crucial role in embryonic dermal lymphatic vascular patterning.

EXPERIMENTAL PROCEDURES

Mice

The *Prox1*$^{GFPCre/+}$ LEC-specific Cre deleter mouse strain (Srinivasan et al., 2010) was kindly provided by Dr. Guillermo Oliver and crossed with

closed-colony Jcl:ICR mice. A colony of mice heterozygous for *PlexinD1*$^{+/-}$ (Gu et al., 2005) or *PlexinD1*$^{flox/+}$ (Zhang et al., 2009) mice was maintained in the C57BL/6 genetic background as described previously. The generation of the *Sema3G*$^{lacZ/+}$ mouse strain is described in the Supplemental Experimental Procedures. 12:00 p.m. on the day when a vaginal plug was observed was considered E0.5. Mice were genotyped by PCR analysis of tail or ear DNA. All animal experiments were approved by the Institutional Animal Care and Use Committee of Kobe University Graduate School of Medicine and carried out in accordance with the animal experimentation guidelines of the Kobe University Graduate School of Medicine.

Antibodies

We used rat anti-PECAM-1 (clone Mec13.3, BD PharMingen), fluorescein isothiocyanate (FITC)-conjugated mouse anti-α-smooth muscle actin (clone 1A4, Sigma), goat anti-Nrp2 (R&D Systems), goat anti-VEGFR3 (R&D), rabbit anti-Cx40 (Alpha Diagnostics), rat anti-MECA32 (BD PharMingen), goat anti-PlexinD1 (R&D), Cy3-conjugated mouse anti-FLAG (clone M2, Sigma), and mouse anti-β-actin (Sigma) antibodies. For immunofluorescence, we used secondary antibodies conjugated to Alexa 488, Cy3, Cy5, or DyLight649 (Life Technologies or Jackson ImmunoResearch).

Immunohistochemistry

For whole-mount preparation, embryos were dissected and fixed overnight with 4% paraformaldehyde (PFA) in PBS at 4°C. The embryos were washed three times with PBS containing 0.2% Triton X-100 (PBT) at 4°C for 30 min, blocked overnight at 4°C in PBT containing 1% BSA, and stained with primary antibodies in blocking solution at 4°C for a week, followed by two vigorous overnight washes in PBT. The samples were incubated with secondary antibodies in blocking solution for another week, followed by two overnight washes in PBT. Stained embryos were dehydrated in methanol and cleared in a mixture of benzyl alcohol and benzyl benzoate (1:2). For flat-mount preparation of the embryonic skin, staining was performed as described previously, except that 1% PFA/PBS was used as fixative (Hirashima et al., 2008). Confocal microscopy was carried out on an Olympus FV-1000 (Olympus) and Zeiss LSM-700 (Carl Zeiss). The artery-lymph arrangement was analyzed as shown in Figure S7. According to a previous report (Li et al., 2013), venous formation was analyzed as average mean fluorescence of MECA32 expression using ImageJ (NIH).

Plasmid Transfection

COS-7 and 293T cells were cultivated in DMEM with 4.5 g/L glucose (Life Technologies), 10% fetal bovine serum (MP Biomedicals), 2 mM L-glutamine (Life Technologies), and penicillin/streptomycin (Life Technologies). 80% confluent COS-7 or 293T cells were transfected with pCAGGS expression vector (Niwa et al., 1991) carrying enhanced GFP, pCMV expression vector carrying mouse PlexinD1 (GenBank: NM_026376), or pcDNA3.1 expression vector (Life Technologies) carrying mouse Nrp2 (isoform 2 precursor, GenBank: NM_001077404) fused to FLAG tag using Lipofectamine 2000 (Life Technologies) according to the manufacturer's instructions. 48 hr after transfection, cells were used for further analyses. To prepare for conditioned medium of Sema-AP proteins, 293T cells were transfected with pAPtag-5 expression vector (GenHunter) carrying mouse Sema3E or mouse Sema3G (Gu et al., 2005; Taniguchi et al., 2005) and cultivated for 7 days in FreeStyle 293 Expression Medium (Life Technologies). The supernatant was concentrated 2-fold by Amicon Ultra-4 50K Centrifugal Filter Devices (Merck Millipore) and used as conditioned medium.

Cell Binding Assay to Sema-AP Proteins

24 hr after transfection with PlexinD1 and/or Nrp2 expression vectors, COS-7 cells were plated at 2×10^5 cells per well in 12-well plates. After another 24 hr, the medium was replaced by conditioned medium containing Sema3E-AP or Sema3G-AP protein. After incubation at 37°C for 30 min, the cells were washed twice with PBS, fixed with 4% PFA/PBS at room temperature for 30 min, and incubated at 65°C for 2 hr to inactivate endogenous AP activity. The cells were equilibrated with 100 mM Tris-HCl (pH 9.5) and then developed with the NBT/BCIP substrate (Nacalai Tesque) at room temperature for 1 hr. Cells binding to Sema-AP proteins were detected as purple cells.

Immunocytochemistry

Cells were fixed with 4% PFA/PBS at 4°C for 20 min, washed three times with PBS at room temperature for 2 min, incubated with PBT at room temperature for 10 min, and washed three times with PBS at room temperature for 2 min. Cells were then blocked in 1% BSA/PBS at room temperature for 1 hr and incubated overnight with primary antibodies in blocking solution at 4°C. Cells were washed three times with PBS at room temperature for 2 min, followed by incubation with secondary antibodies and Alexa-Fluor-633-conjugated phalloidin (Life Technologies) in blocking solution at room temperature for 1 hr. Cells were washed three times with PBS at room temperature for 2 min and analyzed by an inverted microscope (IX81, Olympus). To assess cell collapse induced by semaphorin proteins, images were processed using Photoshop CS5 (Adobe) and cell area was measured by ImageJ. The percentage of cells with area less than 1,600 μm^2 was calculated as presented previously (Gu et al., 2005; Takahashi et al., 1999).

Co-Immunoprecipitation Assay

The 293T cells transfected with vectors expressing PlexinD1 and/or Nrp2 were lysed in 50 mM Tris-HCl (pH 7.5) containing 150 mM NaCl, 5 mM EDTA, 1% Nonidet P-40, and proteinase inhibitor cocktails (Pierce). Total cell extracts were centrifuged at 6,000 × *g* for 15 min, and the supernatant was recovered as the cell lysate. To immunoprecipitate Nrp2-FLAG protein, 1 mg cell lysate was incubated overnight at 4°C with 1 μg anti-FLAG antibody (Sigma) and protein G agarose (GE Healthcare). The immune complexes were then washed three times with lysis buffer, boiled in 2× sample buffer, and loaded on a 7.5% SDS polyacrylamide gel. Western blots were analyzed with anti-PlexinD1, anti-FLAG, or anti-β-actin antibodies and secondary antibodies conjugated to horseradish peroxidase (Jackson ImmunoResearch). To detect the binding between PlexinD1 and Nrp2 endogenous proteins, HMVEC-dLyNeo cells (Lonza) were cultivated in endothelial growth medium 2 (EGM-2) (Bullet Kit, Lonza). The co-immunoprecipitation assay was performed as described above, except that anti-Nrp2 antibody was used for immunoprecipitation.

Wound-Healing Assay

Confluent monolayers of quiescent HMVEC-dLyNeo cells were scratch-wounded, and 20 ng/mL VEGF-C (R&D) and/or conditioned medium containing Sema3G-AP was added. After incubation for 24 hr, wound closure was measured.

Transwell Migration Assay

50,000 HMVEC-dLyNeo cells were placed to the upper chamber of the apparatus (6.5-mm-diameter insert, 3.0-μm pore size; Corning Incorporated) in 100 μL EBM-2 medium (Lonza). 20 ng/mL VEGF-C and/or conditioned medium containing Sema3G-AP was added to the lower chamber in 600 μL EGM-2 (Bullet Kit). After incubation for 48 hr, cells on the lower surface of the membrane were fixed with 3.7% formaldehyde/PBS and stained with hematoxylin. Cells on the upper surface of the membrane were mechanically removed using a cotton swab (Katoh et al., 2006). Migrated cells were counted in six random fields for each membrane.

Statistical Analysis

Values are presented as mean ± SEM. The unpaired two-tailed Student's t test was used to compare results between two groups. One-way ANOVA followed by Tukey-Kramer test was used for multiple comparisons. At least three specimens were analyzed in all cases. p values are indicated as follows: $^{***}p < 0.001$, $^{**}p < 0.01$, and $^{*}p < 0.05$.

SUPPLEMENTAL INFORMATION

Supplemental Information includes Supplemental Experimental Procedures and seven figures and can be found with this article online at http://dx.doi.org/10.1016/j.celrep.2016.11.008.

AUTHOR CONTRIBUTIONS

Conceptualization, M.H.; Methodology, A.U. and M.H.; Investigation, X.L., A.U., Y.F., and M.H.; Resources, Y.Y.; Writing – Original Draft, X.L. and

M.H.; Writing – Review & Editing, X.L., A.U., Y.F., Y.Y., and M.H.; Funding Acquisition, M.H.

ACKNOWLEDGMENTS

We thank Dr. Guillermo Oliver for the *Prox1*$^{GFPCre/+}$ mouse strain, Dr. Christopher Henderson for the *Sema3E*$^{+/-}$ mouse strain, Dr. Jun-ichi Miyazaki for the pCAGGS vector, Dr. Fumikazu Suto for the Nrp2-FLAG vector, Dr. Fanny Mann for the Sema3E-AP vector, and Dr. Masahiko Taniguchi for the Sema3G-AP vector. This study was supported in part by JSPS KAKENHI grant JP26460253 (M.H.) and the Global COE Program "Global Center for Education and Research in Integrative Membrane Biology" (A08) from the Ministry of Education, Culture, Sports, Science and Technology of Japan.

Received: June 25, 2015
Revised: September 12, 2016
Accepted: October 28, 2016
Published: November 22, 2016

REFERENCES

Adams, R.H., and Eichmann, A. (2010). Axon guidance molecules in vascular patterning. Cold Spring Harb. Perspect. Biol. *2*, a001875.

Banu, N., Teichman, J., Dunlap-Brown, M., Villegas, G., and Tufro, A. (2006). Semaphorin 3C regulates endothelial cell function by increasing integrin activity. FASEB J. *20*, 2150–2152.

Bellon, A., Luchino, J., Haigh, K., Rougon, G., Haigh, J., Chauvet, S., and Mann, F. (2010). VEGFR2 (KDR/Flk1) signaling mediates axon growth in response to semaphorin 3E in the developing brain. Neuron *66*, 205–219.

Benedito, R., Roca, C., Sörensen, I., Adams, S., Gossler, A., Fruttiger, M., and Adams, R.H. (2009). The notch ligands Dll4 and Jagged1 have opposing effects on angiogenesis. Cell *137*, 1124–1135.

Bielenberg, D.R., Hida, Y., Shimizu, A., Kaipainen, A., Kreuter, M., Kim, C.C., and Klagsbrun, M. (2004). Semaphorin 3F, a chemorepulsant for endothelial cells, induces a poorly vascularized, encapsulated, nonmetastatic tumor phenotype. J. Clin. Invest. *114*, 1260–1271.

Bouvrée, K., Brunet, I., Del Toro, R., Gordon, E., Prahst, C., Cristofaro, B., Mathivet, T., Xu, Y., Soueid, J., Fortuna, V., et al. (2012). Semaphorin3A, Neuropilin-1, and PlexinA1 are required for lymphatic valve formation. Circ. Res. *111*, 437–445.

Bron, R., Vermeren, M., Kokot, N., Andrews, W., Little, G.E., Mitchell, K.J., and Cohen, J. (2007). Boundary cap cells constrain spinal motor neuron somal migration at motor exit points by a semaphorin-plexin mechanism. Neural Dev. *2*, 21.

Bussmann, J., Bos, F.L., Urasaki, A., Kawakami, K., Duckers, H.J., and Schulte-Merker, S. (2010). Arteries provide essential guidance cues for lymphatic endothelial cells in the zebrafish trunk. Development *137*, 2653–2657.

Carmeliet, P., and Tessier-Lavigne, M. (2005). Common mechanisms of nerve and blood vessel wiring. Nature *436*, 193–200.

Cha, Y.R., Fujita, M., Butler, M., Isogai, S., Kochhan, E., Siekmann, A.F., and Weinstein, B.M. (2012). Chemokine signaling directs trunk lymphatic network formation along the preexisting blood vasculature. Dev. Cell *22*, 824–836.

Chauvet, S., Cohen, S., Yoshida, Y., Fekrane, L., Livet, J., Gayet, O., Segu, L., Buhot, M.C., Jessell, T.M., Henderson, C.E., and Mann, F. (2007). Gating of Sema3E/PlexinD1 signaling by neuropilin-1 switches axonal repulsion to attraction during brain development. Neuron *56*, 807–822.

Chen, H., Chédotal, A., He, Z., Goodman, C.S., and Tessier-Lavigne, M. (1997). Neuropilin-2, a novel member of the neuropilin family, is a high affinity receptor for the semaphorins Sema E and Sema IV but not Sema III. Neuron *19*, 547–559.

Eichmann, A., Makinen, T., and Alitalo, K. (2005). Neural guidance molecules regulate vascular remodeling and vessel navigation. Genes Dev. *19*, 1013–1021.

François, M., Caprini, A., Hosking, B., Orsenigo, F., Wilhelm, D., Browne, C., Paavonen, K., Karnezis, T., Shayan, R., Downes, M., et al. (2008). Sox18 induces development of the lymphatic vasculature in mice. Nature *456*, 643–647.

François, M., Short, K., Secker, G.A., Combes, A., Schwarz, Q., Davidson, T.L., Smyth, I., Hong, Y.K., Harvey, N.L., and Koopman, P. (2012). Segmental territories along the cardinal veins generate lymph sacs via a ballooning mechanism during embryonic lymphangiogenesis in mice. Dev. Biol. *364*, 89–98.

Fukushima, Y., Okada, M., Kataoka, H., Hirashima, M., Yoshida, Y., Mann, F., Gomi, F., Nishida, K., Nishikawa, S., and Uemura, A. (2011). Sema3E-PlexinD1 signaling selectively suppresses disoriented angiogenesis in ischemic retinopathy in mice. J. Clin. Invest. *121*, 1974–1985.

Gaur, P., Bielenberg, D.R., Samuel, S., Bose, D., Zhou, Y., Gray, M.J., Dallas, N.A., Fan, F., Xia, L., Lu, J., and Ellis, L.M. (2009). Role of class 3 semaphorins and their receptors in tumor growth and angiogenesis. Clin. Cancer Res. *15*, 6763–6770.

Gitler, A.D., Lu, M.M., and Epstein, J.A. (2004). PlexinD1 and semaphorin signaling are required in endothelial cells for cardiovascular development. Dev. Cell *7*, 107–116.

Grandclement, C., Pallandre, J.R., Valmary Degano, S., Viel, E., Bouard, A., Balland, J., Rémy-Martin, J.P., Simon, B., Rouleau, A., Boireau, W., et al. (2011). Neuropilin-2 expression promotes TGF-β1-mediated epithelial to mesenchymal transition in colorectal cancer cells. PLoS ONE *6*, e20444.

Gu, C., Yoshida, Y., Livet, J., Reimert, D.V., Mann, F., Merte, J., Henderson, C.E., Jessell, T.M., Kolodkin, A.L., and Ginty, D.D. (2005). Semaphorin 3E and plexin-D1 control vascular pattern independently of neuropilins. Science *307*, 265–268.

Gurrapu, S., and Tamagnone, L. (2016). Transmembrane semaphorins: multimodal signaling cues in development and cancer. Cell Adhes. Migr. Published online June 13, 2016. http://dx.doi.org/10.1080/19336918.2016.1197479.

Guttmann-Raviv, N., Shraga-Heled, N., Varshavsky, A., Guimaraes-Sternberg, C., Kessler, O., and Neufeld, G. (2007). Semaphorin-3A and semaphorin-3F work together to repel endothelial cells and to inhibit their survival by induction of apoptosis. J. Biol. Chem. *282*, 26294–26305.

Hägerling, R., Pollmann, C., Andreas, M., Schmidt, C., Nurmi, H., Adams, R.H., Alitalo, K., Andresen, V., Schulte-Merker, S., and Kiefer, F. (2013). A novel multistep mechanism for initial lymphangiogenesis in mouse embryos based on ultramicroscopy. EMBO J. *32*, 629–644.

Hirashima, M., Sano, K., Morisada, T., Murakami, K., Rossant, J., and Suda, T. (2008). Lymphatic vessel assembly is impaired in Aspp1-deficient mouse embryos. Dev. Biol. *316*, 149–159.

James, J.M., Nalbandian, A., and Mukouyama, Y.S. (2013). TGFβ signaling is required for sprouting lymphangiogenesis during lymphatic network development in the skin. Development *140*, 3903–3914.

Jongbloets, B.C., and Pasterkamp, R.J. (2014). Semaphorin signalling during development. Development *141*, 3292–3297.

Jurisic, G., Maby-El Hajjami, H., Karaman, S., Ochsenbein, A.M., Alitalo, A., Siddiqui, S.S., Ochoa Pereira, C., Petrova, T.V., and Detmar, M. (2012). An unexpected role of semaphorin3a-neuropilin-1 signaling in lymphatic vessel maturation and valve formation. Circ. Res. *111*, 426–436.

Karayan-Tapon, L., Wager, M., Guilhot, J., Levillain, P., Marquant, C., Clarhaut, J., Potiron, V., and Roche, J. (2008). Semaphorin, neuropilin and VEGF expression in glial tumours: SEMA3G, a prognostic marker? Br. J. Cancer *99*, 1153–1160.

Karkkainen, M.J., Haiko, P., Sainio, K., Partanen, J., Taipale, J., Petrova, T.V., Jeltsch, M., Jackson, D.G., Talikka, M., Rauvala, H., et al. (2004). Vascular endothelial growth factor C is required for sprouting of the first lymphatic vessels from embryonic veins. Nat. Immunol. *5*, 74–80.

Katoh, H., Hiramoto, K., and Negishi, M. (2006). Activation of Rac1 by RhoG regulates cell migration. J. Cell Sci. *119*, 56–65.

Kim, J., Oh, W.J., Gaiano, N., Yoshida, Y., and Gu, C. (2011). Semaphorin 3E-Plexin-D1 signaling regulates VEGF function in developmental angiogenesis via a feedback mechanism. Genes Dev. *25*, 1399–1411.

Koropouli, E., and Kolodkin, A.L. (2014). Semaphorins and the dynamic regulation of synapse assembly, refinement, and function. Curr. Opin. Neurobiol. *27*, 1–7.

Kumanogoh, A., and Kikutani, H. (2013). Immunological functions of the neuropilins and plexins as receptors for semaphorins. Nat. Rev. Immunol. *13*, 802–814.

Kutschera, S., Weber, H., Weick, A., De Smet, F., Genove, G., Takemoto, M., Prahst, C., Riedel, M., Mikelis, C., Baulande, S., et al. (2011). Differential endothelial transcriptomics identifies semaphorin 3G as a vascular class 3 semaphorin. Arterioscler. Thromb. Vasc. Biol. *31*, 151–159.

Li, W., Kohara, H., Uchida, Y., James, J.M., Soneji, K., Cronshaw, D.G., Zou, Y.R., Nagasawa, T., and Mukouyama, Y.S. (2013). Peripheral nerve-derived CXCL12 and VEGF-A regulate the patterning of arterial vessel branching in developing limb skin. Dev. Cell *24*, 359–371.

Mahadevan, A., Welsh, I.C., Sivakumar, A., Gludish, D.W., Shilvock, A.R., Noden, D.M., Huss, D., Lansford, R., and Kurpios, N.A. (2014). The left-right Pitx2 pathway drives organ-specific arterial and lymphatic development in the intestine. Dev. Cell *31*, 690–706.

Martinez-Corral, I., Ulvmar, M.H., Stanczuk, L., Tatin, F., Kizhatil, K., John, S.W., Alitalo, K., Ortega, S., and Makinen, T. (2015). Nonvenous origin of dermal lymphatic vasculature. Circ. Res. *116*, 1649–1654.

Meadows, S.M., and Cleaver, O. (2015). Vascular patterning: coordinated signals keep blood vessels on track. Curr. Opin. Genet. Dev. *32*, 86–91.

Meadows, S.M., Fletcher, P.J., Moran, C., Xu, K., Neufeld, G., Chauvet, S., Mann, F., Krieg, P.A., and Cleaver, O. (2012). Integration of repulsive guidance cues generates avascular zones that shape mammalian blood vessels. Circ. Res. *110*, 34–46.

Mukouyama, Y.S., Shin, D., Britsch, S., Taniguchi, M., and Anderson, D.J. (2002). Sensory nerves determine the pattern of arterial differentiation and blood vessel branching in the skin. Cell *109*, 693–705.

Neufeld, G., and Kessler, O. (2008). The semaphorins: versatile regulators of tumour progression and tumour angiogenesis. Nat. Rev. Cancer *8*, 632–645.

Niwa, H., Yamamura, K., and Miyazaki, J. (1991). Efficient selection for high-expression transfectants with a novel eukaryotic vector. Gene *108*, 193–199.

Nurmi, H., Saharinen, P., Zarkada, G., Zheng, W., Robciuc, M.R., and Alitalo, K. (2015). VEGF-C is required for intestinal lymphatic vessel maintenance and lipid absorption. EMBO Mol. Med. *7*, 1418–1425.

Ou, J.J., Wei, X., Peng, Y., Zha, L., Zhou, R.B., Shi, H., Zhou, Q., and Liang, H.J. (2015). Neuropilin-2 mediates lymphangiogenesis of colorectal carcinoma via a VEGFC/VEGFR3 independent signaling. Cancer Lett. *358*, 200–209.

Ruediger, T., Zimmer, G., Barchmann, S., Castellani, V., Bagnard, D., and Bolz, J. (2013). Integration of opposing semaphorin guidance cues in cortical axons. Cereb. Cortex *23*, 604–614.

Sabin, F.R. (1902). On the origin of the lymphatic system from the veins and the development of the lymph hearts and thoracic ductin the pig. Am. J. Anat. *1*, 367–389.

Sabin, F.R. (1904). On the development of the superficial lymphatics in the skin of the pig. Am. J. Anat. *3*, 183–195.

Srinivasan, R.S., Dillard, M.E., Lagutin, O.V., Lin, F.J., Tsai, S., Tsai, M.J., Samokhvalov, I.M., and Oliver, G. (2007). Lineage tracing demonstrates the venous origin of the mammalian lymphatic vasculature. Genes Dev. *21*, 2422–2432.

Srinivasan, R.S., Geng, X., Yang, Y., Wang, Y., Mukatira, S., Studer, M., Porto, M.P., Lagutin, O., and Oliver, G. (2010). The nuclear hormone receptor Coup-TFII is required for the initiation and early maintenance of Prox1 expression in lymphatic endothelial cells. Genes Dev. *24*, 696–707.

Stanczuk, L., Martinez-Corral, I., Ulvmar, M.H., Zhang, Y., Laviña, B., Fruttiger, M., Adams, R.H., Saur, D., Betsholtz, C., Ortega, S., et al. (2015). cKit lineage hemogenic endothelium-derived cells contribute to mesenteric lymphatic vessels. Cell Rep. *10*, 1708–1721.

Sulpice, E., Plouët, J., Bergé, M., Allanic, D., Tobelem, G., and Merkulova-Rainon, T. (2008). Neuropilin-1 and neuropilin-2 act as coreceptors, potentiating proangiogenic activity. Blood *111*, 2036–2045.

Swift, M.R., and Weinstein, B.M. (2009). Arterial-venous specification during development. Circ. Res. *104*, 576–588.

Takahashi, T., Nakamura, F., Jin, Z., Kalb, R.G., and Strittmatter, S.M. (1998). Semaphorins A and E act as antagonists of neuropilin-1 and agonists of neuropilin-2 receptors. Nat. Neurosci. *1*, 487–493.

Takahashi, T., Fournier, A., Nakamura, F., Wang, L.H., Murakami, Y., Kalb, R.G., Fujisawa, H., and Strittmatter, S.M. (1999). Plexin-neuropilin-1 complexes form functional semaphorin-3A receptors. Cell *99*, 59–69.

Tammela, T., and Alitalo, K. (2010). Lymphangiogenesis: molecular mechanisms and future promise. Cell *140*, 460–476.

Taniguchi, M., Masuda, T., Fukaya, M., Kataoka, H., Mishina, M., Yaginuma, H., Watanabe, M., and Shimizu, T. (2005). Identification and characterization of a novel member of murine semaphorin family. Genes Cells *10*, 785–792.

Tata, A., Stoppel, D.C., Hong, S., Ben-Zvi, A., Xie, T., and Gu, C. (2014). An image-based RNAi screen identifies SH3BP1 as a key effector of Semaphorin 3E-PlexinD1 signaling. J. Cell Biol. *205*, 573–590.

Torres-Vázquez, J., Gitler, A.D., Fraser, S.D., Berk, J.D., Fishman, M.C., Childs, S., Epstein, J.A., and Weinstein, B.M.; Van N Pham (2004). Semaphorin-plexin signaling guides patterning of the developing vasculature. Dev. Cell *7*, 117–123.

Tran, T.S., Kolodkin, A.L., and Bharadwaj, R. (2007). Semaphorin regulation of cellular morphology. Annu. Rev. Cell Dev. Biol. *23*, 263–292.

Uchida, Y., James, J.M., Suto, F., and Mukouyama, Y.S. (2015). Class 3 semaphorins negatively regulate dermal lymphatic network formation. Biol. Open *4*, 1194–1205.

Wigle, J.T., Harvey, N., Detmar, M., Lagutina, I., Grosveld, G., Gunn, M.D., Jackson, D.G., and Oliver, G. (2002). An essential role for Prox1 in the induction of the lymphatic endothelial cell phenotype. EMBO J. *21*, 1505–1513.

Xu, Y., Yuan, L., Mak, J., Pardanaud, L., Caunt, M., Kasman, I., Larrivée, B., Del Toro, R., Suchting, S., Medvinsky, A., et al. (2010). Neuropilin-2 mediates VEGF-C-induced lymphatic sprouting together with VEGFR3. J. Cell Biol. *188*, 115–130.

Yaniv, K., Isogai, S., Castranova, D., Dye, L., Hitomi, J., and Weinstein, B.M. (2006). Live imaging of lymphatic development in the zebrafish. Nat. Med. *12*, 711–716.

Yoshida, Y. (2012). Semaphorin signaling in vertebrate neural circuit assembly. Front. Mol. Neurosci. *5*, 71.

Yuan, L., Moyon, D., Pardanaud, L., Bréant, C., Karkkainen, M.J., Alitalo, K., and Eichmann, A. (2002). Abnormal lymphatic vessel development in neuropilin 2 mutant mice. Development *129*, 4797–4806.

Zhang, Y., Singh, M.K., Degenhardt, K.R., Lu, M.M., Bennett, J., Yoshida, Y., and Epstein, J.A. (2009). Tie2Cre-mediated inactivation of plexinD1 results in congenital heart, vascular and skeletal defects. Dev. Biol. *325*, 82–93.

Cell Reports, Volume *17*

Supplemental Information

Semaphorin 3G Provides a Repulsive Guidance Cue to Lymphatic Endothelial Cells via Neuropilin-2/PlexinD1

Xinyi Liu, Akiyoshi Uemura, Yoko Fukushima, Yutaka Yoshida, and Masanori Hirashima

SUPPLEMENTAL FIGURES AND LEGENDS

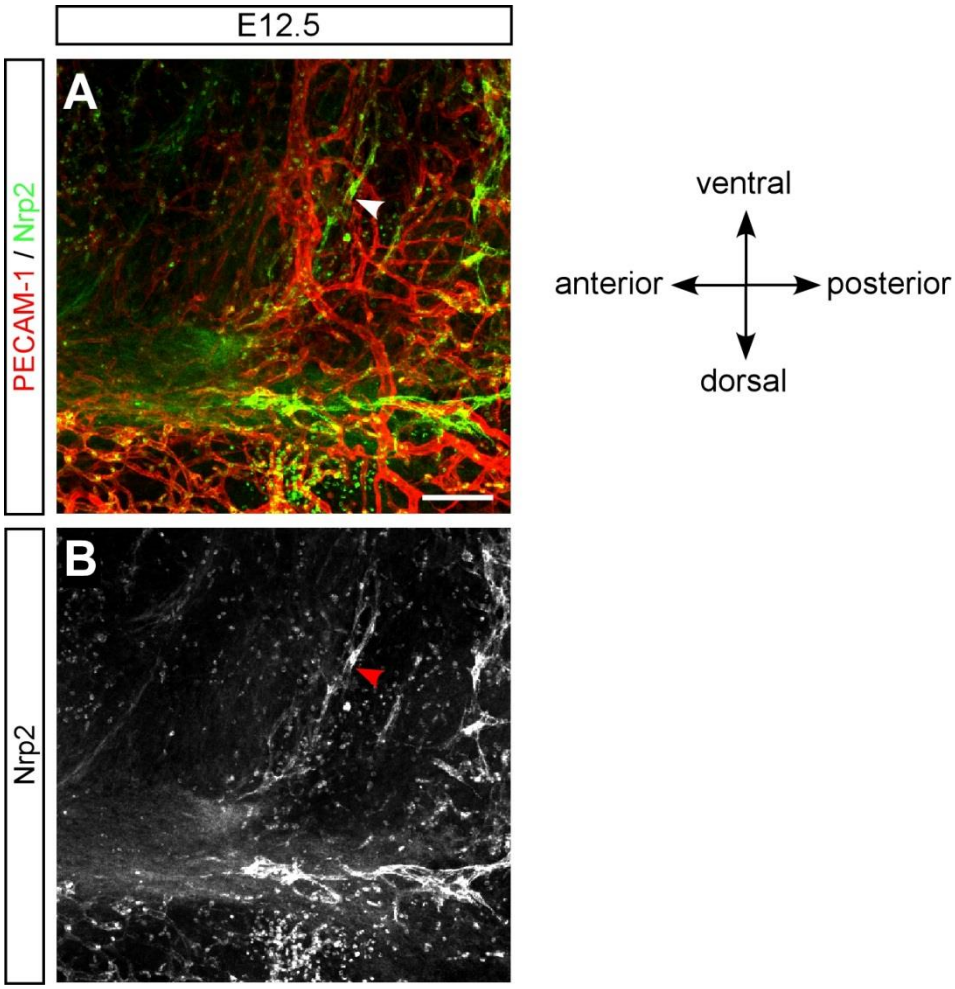

Figure S1. Lymphatic vascular formation in mouse embryonic skin initiates on the lateral side of embryos, Related to Figure 1. Whole-mount immunohistochemistry of a mouse embryo is shown in lateral view for PECAM-1 (A, red) and Nrp2 (A, green; B, white) at E12.5. Nrp2^{+} LECs (arrowhead) are seen in the skin between the cervical and thoracic area. Scale bars, 100 μm.

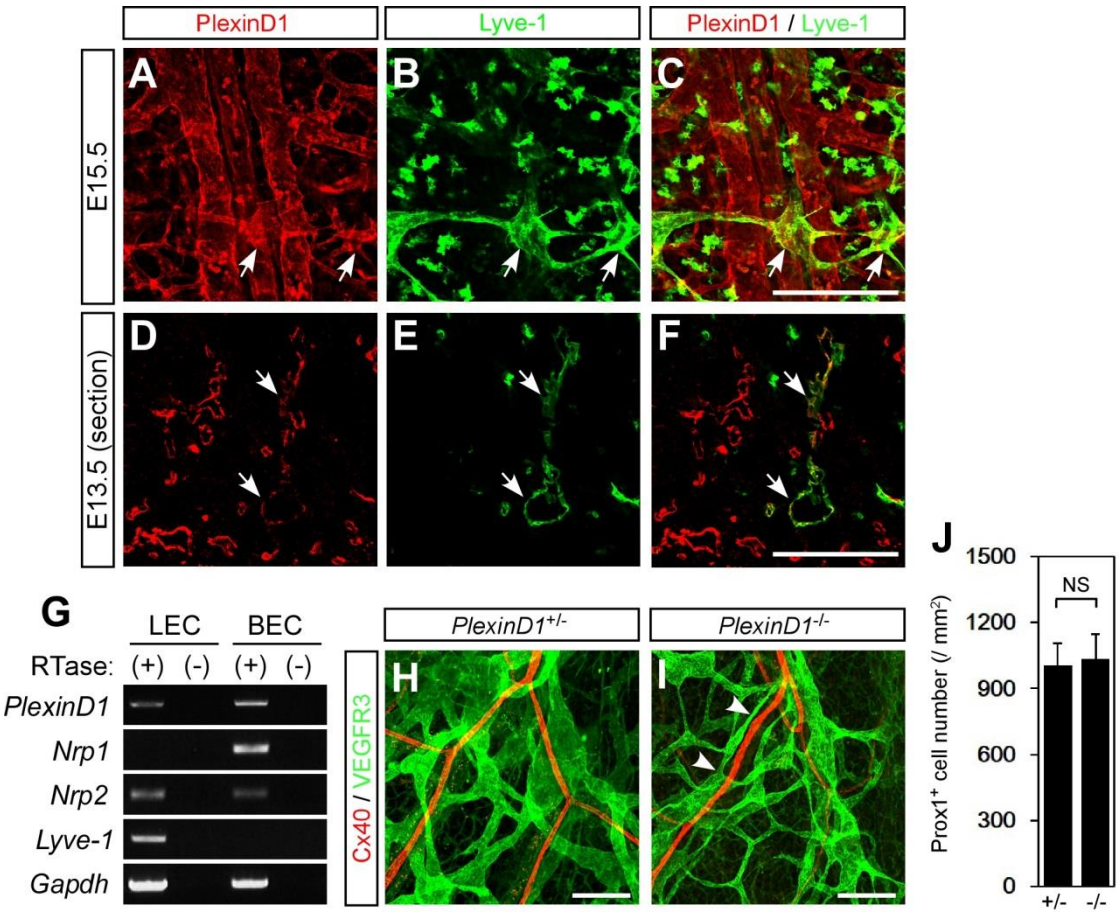

Figure S2. PlexinD1 is expressed in LECs and BECs, Related to Figure 2. (A–F) Immunohistochemistry of whole-mount (A–C, at E15.5) or transverse section (D–F, at E13.5) of back skin is shown for PlexinD1 (red) and Lyve-1 (green). PlexinD1 is expressed in Lyve-1^{+} lymphatic vessels (arrows) as well as blood vessels. (G) RT-PCR analysis using LECs and BECs purified from mouse embryonic back skin at E14.5. (H, I) Whole-mount immunohistochemistry of back skin is shown for Cx40 (red), and VEGFR3 (green) at E15.5. VEGFR3^{+} lymphatic vessels are tightly associated with Cx40^{+} arteries in *PlexinD1*$^{-/-}$ embryos (arrowheads). (J) Statistical analysis of Prox1^{+} LEC number in embryo back skin at E15.5. The number of LECs are comparable between *PlexinD1*$^{+/-}$ and *PlexinD1*$^{-/-}$ embryos (n =4 each group). Values are presented as mean ± SEM. NS, not significant, unpaired two-tailed Student's *t*-test. Scale bars, 100 μm.

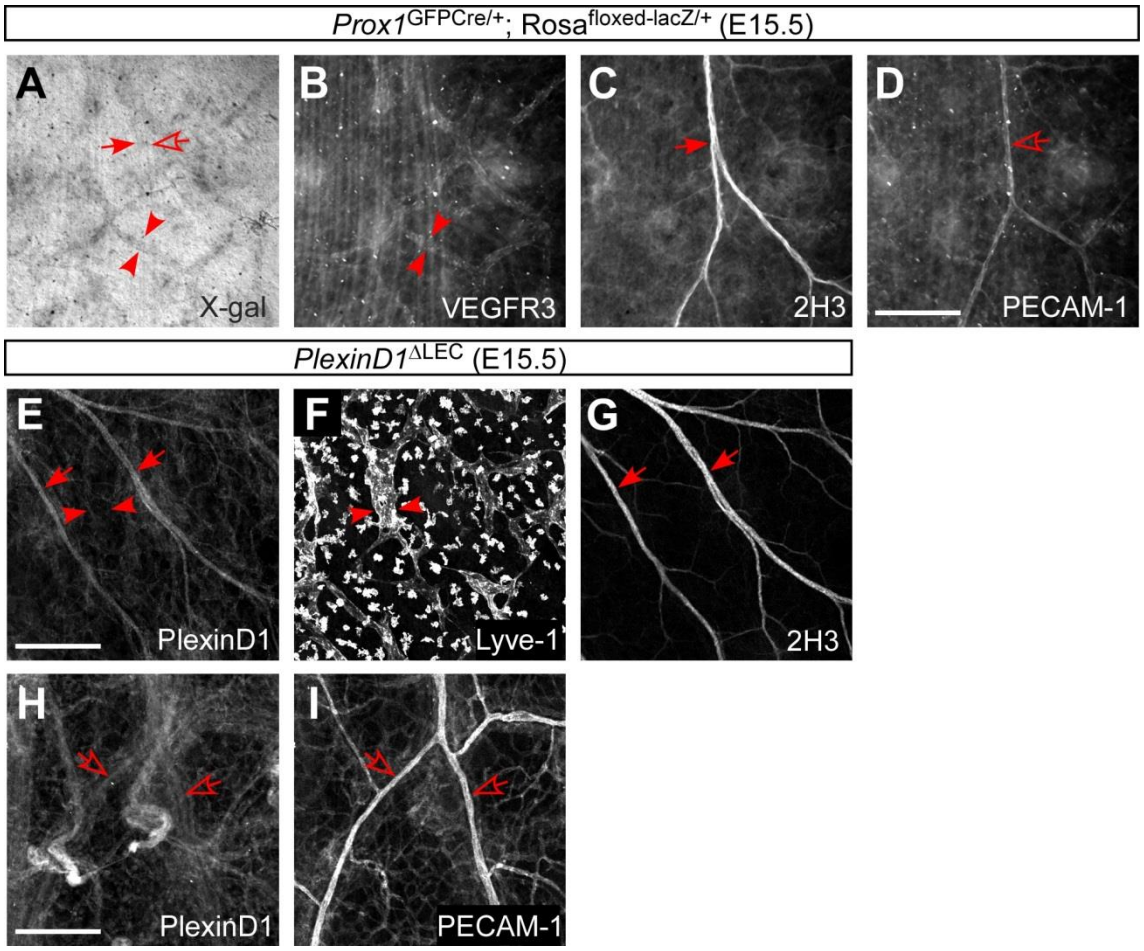

Figure S3. *PlexinD1*$^{\Delta LEC}$ embryos were generated by using *Prox1*$^{GFPCre/+}$ mouse strain, Related to Figure 3. (A–D) X-gal staining (A, black) and immunohistochemistry for VEGFR3 (B, white), 2H3 (C, white), and PECAM-1 (D, white) of *Prox1*$^{GFPCre/+}$; *Rosa26*$^{floxed\text{-}lacZ/+}$ mouse embryonic back skin identified the Cre recombinase activity in lymphatic vessels (arrowheads) but not in neurons (arrow) or blood vessels (open arrow) at E15.5. (E–I) Whole-mount immunohistochemistry of *PlexinD1*$^{\Delta LEC}$ embryonic back skin is shown for PlexinD1 (E, H), Lyve-1 (F), 2H3 (G), and PECAM-1 (I) at E15.5. PlexinD1 expression is lost in lymphatic vessels (arrowheads) but is still present in neurons (arrows) and blood vessels (open arrows) of *PlexinD1*$^{\Delta LEC}$ embryos. Scale bars, 100 μm.

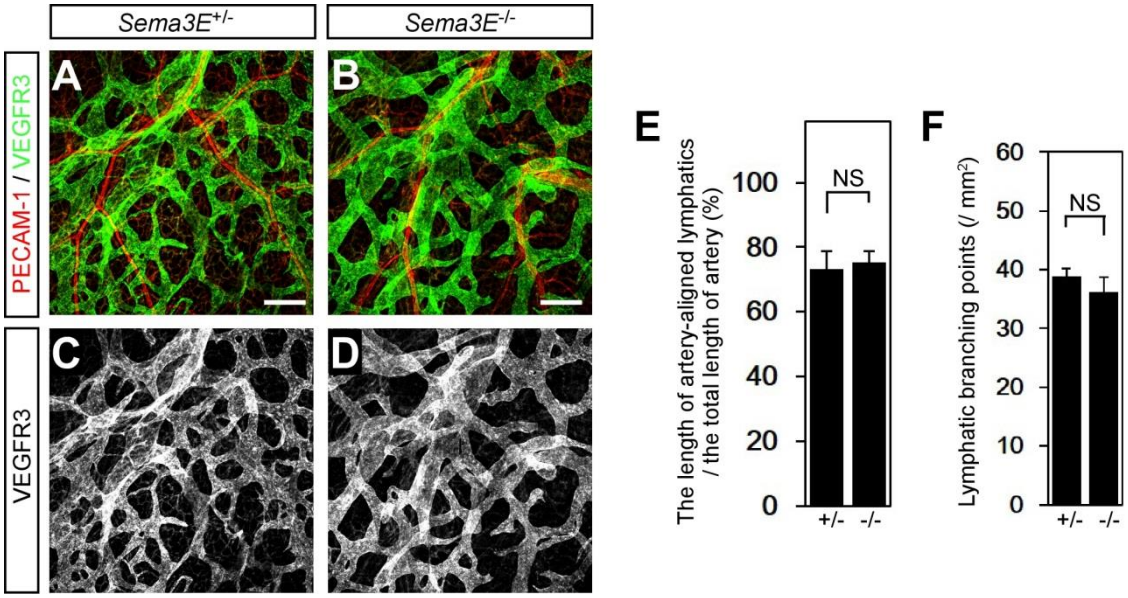

Figure S4. *Sema3E*$^{-/-}$ embryos showed a normal lymphatic vascular patterning in mouse embryonic back skin, Related to Figure 4. Whole-mount immunohistochemistry of back skin is shown for PECAM-1 (A, B, red) and VEGFR3 (A, B, green; C, D, white) at E15.5. Lymphatic vessels form a random network with a pattern that is not related to blood vessels in *Sema3E*$^{-/-}$ embryos. Statistical analyses of artery-lymph arrangement (E) and lymphatic branching (F) (n =3 each group). Values are presented as mean ± SEM. NS, not significant, unpaired two-tailed Student's *t*-test. Scale bars, 100 μm.

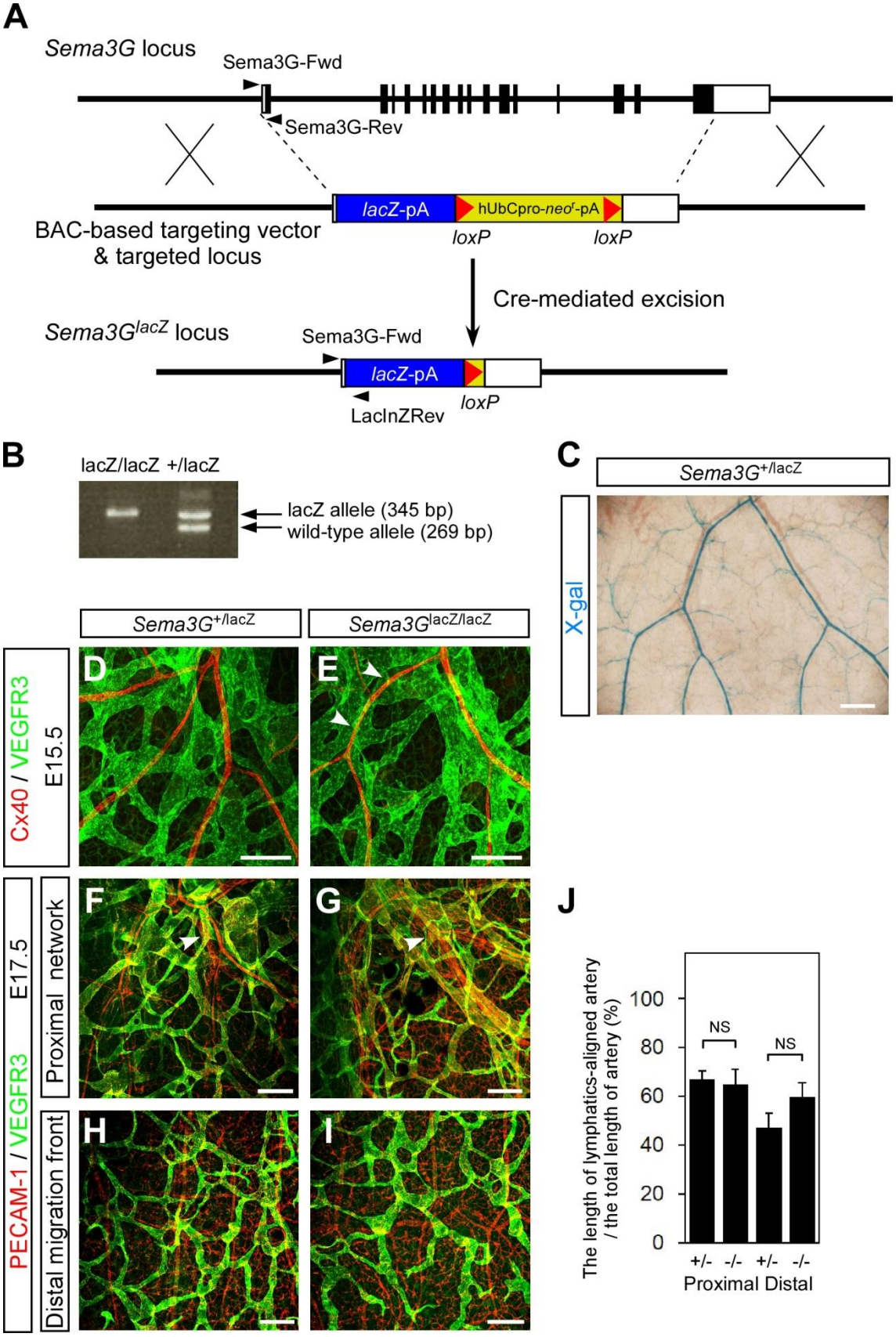
A
Sema3G locus
Sema3G-Fwd
Sema3G-Rev
lacZ-pA
hUbCpro-neo^r-pA
BAC-based targeting vector
& targeted locus
loxP
loxP
Cre-mediated excision
Sema3G^lacZ locus
Sema3G-Fwd
lacZ-pA
LacInZRev
loxP
B
lacZ/lacZ +/lacZ
lacZ allele (345 bp)
wild-type allele (269 bp)
C
Sema3G+/lacZ
X-gal
Sema3G+/lacZ
Sema3GlacZ/lacZ
Cx40 / VEGFR3
E15.5
D
E
PECAM-1 / VEGFR3
E17.5
Proximal network
F
G
Distal migration front
H
I
J
The length of lymphatics-aligned artery / the total length of artery (%)
100
80
60
40
20
0
NS
NS
+/-
-/-
+/-
-/-
Proximal
Distal

Figure S5. Generation and analysis of *Sema3G*$^{lacZ/lacZ}$ mice, Related to Figure 4. (A) Schematic representation of *Sema3G* gene targeting strategy. The genomic sequence carrying the whole coding sequence of the *Sema3G* gene was replaced with a lacZ/neo cassette by homologous recombination using a bacterial artificial chromosome (BAC)-based targeting vector. The floxed neo cassette was removed by Cre-mediated excision to obtain the *Sema3G*^{lacZ} allele. Exons and untranslated regions are shown as filled and open boxes, respectively. (B) PCR genotyping with Sema3G-Fwd, Sema3G-Rev, and LacInZRev primers shown as arrowheads in panel A. (C) X-gal staining of *Sema3G*$^{+/lacZ}$ mouse embryonic back skin identified the preferential expression in arteries at E15.5. (D, E) Whole-mount immunohistochemistry of back skin is shown for Cx40 (red) and VEGFR3 (green) at E15.5. VEGFR3^{+} lymphatic vessels are tightly associated with Cx40^{+} arteries in *Sema3G*$^{lacZ/lacZ}$ embryos (arrowheads). (F–I) Whole-mount immunohistochemistry of back skin is shown for PECAM-1 (red) and VEGFR3 (green) at E17.5. Lymphatic vessels form a random network whose pattern is not related to blood vessels in Sema3G$^{lacZ/lacZ}$, compared to control littermates. (J) Statistical analysis of artery-lymph arrangement at E17.5 (*Sema3G*$^{+/lacZ}$, n = 3; *Sema3G*$^{lacZ/lacZ}$, n = 6). Values are presented as mean ± SEM. NS, not significant, unpaired two-tailed Student's *t*-test. Scale bars, 100 μm.

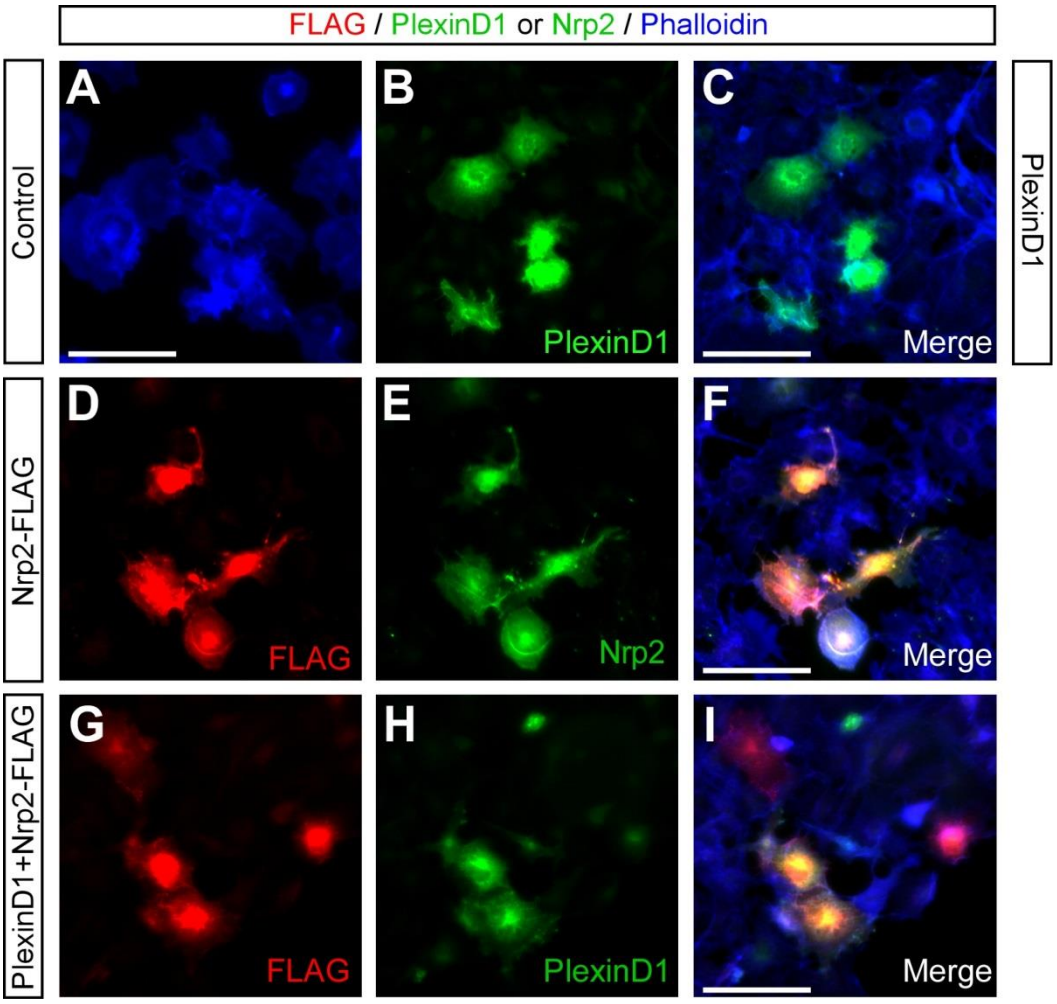

Figure S6. Morphology of transfected COS-7 cells under non-stimulated conditions, Related to Figure 6. Immunocytochemistry of COS-7 cells is shown after being transfected with expression vectors carrying PlexinD1 (B–C), Nrp2-FLAG (D–F), or both (G–I), and stained by using antibodies to PlexinD1 (B, C, H, I, green), FLAG (D, F, G, I, red), and Nrp2 (E, F, green), and phalloidin (A, C, F, I, blue). Scale bars, 100 μm.

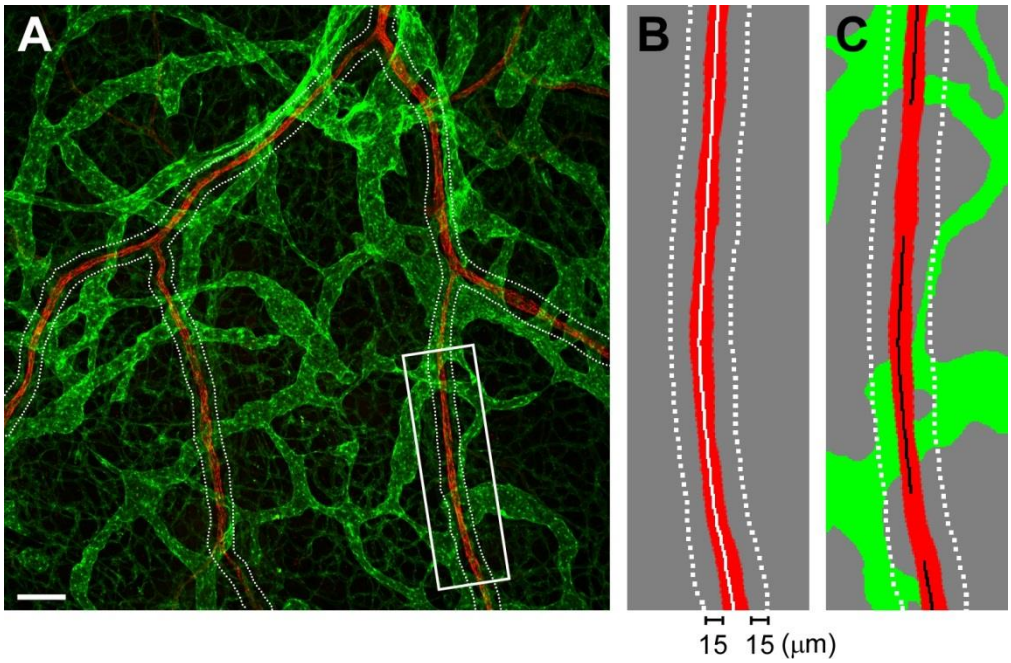

Figure S7. Schematic representation of measurement of artery-lymph arrangement, Related to Figure 2–4, S4–S5. (A) Whole-mount immunohistochemistry of back skin is shown for arterial endothelial marker Cx40 (red) and LEC marker VEGFR3 (green) at E15.5. Scale bars, 100 μm. Area of rectangle is shown in B and C. Artery-lymph arrangement was assessed by the following methods. (B) Center line of artery (red) is drawn in white. (C) In the area within two dashed lines (15 μm from the edge of arteries), center line of artery is colored in black or erased where adjacent lymphatic vessels (green) are present or absent, respectively. The length of lymphatics-aligned artery per the total length of artery (%) was calculated as total length of black line per total length of white line. Images were processed using Photoshop CS5 and total length of lines was measured by ImageJ.

SUPPLEMENTAL EXPERIMENTAL PROCEDURES

Antibodies

We used rabbit anti-Lyve-1 (Reliatech), rabbit anti-Prox1 (Covance), and mouse anti-neurofilament (clone 2H3, Developmental Studies Hybridoma Bank) antibodies.

Immunohistochemistry of Cryosections

Embryos were dissected at E13.5, embedded in OCT compound, and cut transversely into 10 μm sections. Following fixation in 4% PFA/PBS, sections were stained, as described previously (Hirashima et al., 2008).

RT-PCR

PECAM-1^{+}/Lyve-1^{+}/CD45^{-} LECs and PECAM-1^{+}/Lyve-1^{-}/CD45^{-} BECs from E14.5 mouse embryonic back skin were purified by fluorescence-activated cell sorting, as described previously (Hirashima et al., 2008). Total RNA was isolated from purified cells using Trizol (Invitrogen), according to the manufacturer's instructions. One mg of total RNA was reverse-transcribed using the SuperScript first-strand synthesis system for RT-PCR (Invitrogen). Control specimens were prepared without reverse transcriptase (RTase). First-strand cDNA was used for PCR with specific primers for *PlexinD1* (forward, 5'-TGCAGAAGAGTGACCAGGAG-3'; reverse, 5'-AAGTGGTGCTCTTTAGAAAC-3'), *Nrp1* (forward, 5'-ACTGACAGCGCAATAGCAAAAGAAG-3'; reverse, 5'-TCGGACAAATCGAGTTATCAGTGGT-3'), *Nrp2* (forward, 5'-TGTTCGAGGGAGTGATAGGG-3'; reverse, 5'-CAGAAGCGATCCAGACACAA-3'), *Lyve-1* (forward, 5'-TTCCTCGCCTCTATTTGGAC-3'; reverse, 5'-ACGGGGTAAAATGTGGTAAC-3'), and *Gapdh* (forward, 5'-AAGGTCGGTGTGAACGGATTTGGC- 3'; reverse, 5'-AAGGTGGAAGAGTGGGAGTTGCTG-3').

Measurement of LEC number

Whole-mount double fluorescence confocal microscopy of embryonic back skin using antibodies to Prox1 and VEGFR3 at E15.5 was performed, and the number of Prox1^{+} LEC nuclei was counted. The number per analyzed area of skin is presented.

Mice

Sema3E$^{+/-}$ (Gu et al., 2005) strain was obtained from the European Mutant Mouse Archive (EMMA). EIIa-Cre deleter (Lakso et al., 1996) and *Rosa26*$^{\text{floxed-lacZ/+}}$ (Soriano, 1999) Cre reporter strains were obtained from the Jackson Laboratory. A colony of mice heterozygous for *Sema3E*$^{+/-}$, EIIa-Cre, or *Rosa26*$^{\text{floxed-lacZ/+}}$ was maintained in the C57BL/6 genetic background as described previously. For

Sema3G-deficient mice, *Sema3G*$^{tm1(KOMP)Vlcg}$ mouse strain generated by VelociGene (project ID: VG10084) (Valenzuela et al., 2003) was obtained from the Knockout Mouse Project (KOMP) Repository. The floxed hUbCpro-*neo*^{r}-pA cassette was removed by crossing with an EIIa-Cre deleter strain, and the EIIa-Cre allele was removed by crossing with C57BL/6 mice before phenotypic analysis of *Sema3G*-deficient mice. We designate heterozygous mice carrying the targeted locus without hUbCpro-*neo*^{r}-pA cassette as *Sema3G*$^{lacZ/+}$. Genotyping of *Sema3G*$^{lacZ/+}$ mice was performed by PCR analysis of tail DNA or yolk sac at an annealing temperature of 65°C with the following primers, Sema3G-Fwd, 5'-TAGCTGCACGGGCATTGAGC-3'; Sema3G-Rev, 5'-CCCACATGGAACAGAAGGCT-3'; and LacInZRev, 5'-GTCTGTCCTAGCTTCCTCACTG-3'. The wild-type allele gave a 269-bp band, whereas the mutant allele gave a 345-bp band. The following primers were used for the genotyping of neo (neo-Fwd, 5'-CGGCTATGACTGGGCACAACAGAC-3' and neo-Rev, 5'-CTTCGTCCAGATCATCCTGATCGAC-3'; 422-bp band), and Cre (Cre-Fwd, 5'-AAATTGCCAGGATCAGGGTTAAAG-3' and Cre-Rev, 5'-AGAGTCATCCTTAGCGCCGTAAAT-3'; 311-bp band).

X-gal Staining

Whole-mount embryos were dissected and fixed overnight in 100 mM sodium phosphate (pH 7.3) with 2 mM $MgCl_2$ (basal buffer) containing 0.2% glutaraldehyde and 5 mM ethylenediaminetetraacetic acid at 4°C. Back skin was peeled off and further fixed at 4°C for 3 h. For X-gal staining followed by immunohistochemistry, whole-mount embryos were fixed in 1% PFA/PBS for 1 h at 4°C and back skin was peeled off. The specimens were washed three times with basal buffer containing 0.02% Nonidet P-40 at room temperature for 15 min, and then developed overnight with basal buffer containing 1 mg/ml 5-bromo-4-chloro-3-indolyl-β-D-galactoside (Nacalai tesque), 5 mM potassium ferrocyanide, and 5 mM potassium ferricyanide at 4°C. Stained back skins were flat-mounted on slide glasses and analyzed by IX81 (Olympus). Background staining was minimal in wild-type control back skin (data not shown).

SUPPLEMENTAL REFERENCES

Lakso, M., Pichel, J.G., Gorman, J.R., Sauer, B., Okamoto, Y., Lee, E., Alt, F.W., and Westphal, H. (1996). Efficient in vivo manipulation of mouse genomic sequences at the zygote stage. Proc Natl Acad Sci U S A *93*, 5860-5865.

Soriano, P. (1999). Generalized lacZ expression with the ROSA26 Cre reporter strain. Nat Genet *21*, 70-71.

Valenzuela, D.M., Murphy, A.J., Frendewey, D., Gale, N.W., Economides, A.N., Auerbach, W., Poueymirou, W.T., Adams, N.C., Rojas, J., Yasenchak, J., *et al.* (2003). High-throughput engineering of the mouse genome coupled with high-resolution expression analysis. Nat Biotechnol *21*, 652-659.